



# Exploring the inhibitory effect of H<sub>2</sub>O on CO<sub>2</sub>/CH<sub>4</sub> adsorption in coal: Insights from experimental and simulation approaches



Hongmin Yang <sup>a,b,c</sup>, Ningning Kang <sup>a</sup>, Xiangjun Chen <sup>a,b,d,\*</sup>, Yuan Liu <sup>a</sup>

<sup>a</sup> College of Safety Science and Engineering (Henan Polytechnic University), Jiaozuo, 454003, China

<sup>b</sup> State Collaborative Innovation Center of Coal Work Safety and Clean-efficiency Utilization (Henan Polytechnic University), Jiaozuo, 454003, China

<sup>c</sup> Engineer Research Center of Minister of Education for Coal Mine Disaster Prevention and Emergency Relief (Henan Polytechnic University), Jiaozuo, 454003, China

<sup>d</sup> State Key Laboratory Cultivation Base for Gas Geology and Gas Control (Henan Polytechnic University), Jiaozuo, 454003, China

## ARTICLE INFO

Handling editor: Wojciech Stanek

### Keywords:

Anthracite  
Moisture influence coefficient  
Adsorption properties  
Interaction energy  
Oxygen-containing functional groups  
Hydrogen bond

## ABSTRACT

To investigate the inhibitory effect of H<sub>2</sub>O on the adsorption of CH<sub>4</sub>/CO<sub>2</sub> in coal, the anthracite was selected for physical adsorption experiments on CH<sub>4</sub>/CO<sub>2</sub> gases in this study. Combined with Materials Studio software, the effect of moisture on the isothermal adsorption characteristics of CH<sub>4</sub>/CO<sub>2</sub> in coal was investigated by using density functional theory and giant canonical Monte Carlo simulation. The intermolecular interaction energies were obtained, as well as the effects of electrostatic potentials, adsorption sites, and hydrogen bonding of oxygen-containing functional groups. The results show that: ① According to the CH<sub>4</sub>/CO<sub>2</sub> isothermal adsorption experiments, it was found that moisture significantly inhibited the adsorption of CH<sub>4</sub>/CO<sub>2</sub> by coal. For CH<sub>4</sub>, the relationship between adsorption constants a/b and moisture content can be expressed by the equations  $y = 43.447 - 3.348x$  and  $y = 3.225 - 0.751x$ . For CO<sub>2</sub>, adsorption constant a follows a power function relationship with moisture content, expressed as  $y = 29.114x^{-0.063}$ , while adsorption constant b is represented by the polynomial fitting equation  $y = 1.672 + 0.508x + 0.083x^2$ . ② The findings have revealed correlations between the moisture influence coefficient and moisture content. The exponential functional equation  $\eta = \exp(-0.188\omega)$  was found to be more accurate for coal adsorbing CH<sub>4</sub>, whereas the linear functional equation  $\eta = 1/(1 + 0.243\omega)$  was considered more appropriate for CO<sub>2</sub>. ③ The van der Waals and electrostatic energies between coal and CH<sub>4</sub>/CO<sub>2</sub> decreased with an increase in moisture content, whereas the van der Waals and electrostatic energies between coal and H<sub>2</sub>O increased. ④ The orders of hydrogen bond formation ability between CH<sub>4</sub>/CO<sub>2</sub> and functional groups were as follows: -CHO > -COOH > -OH > -CH<sub>3</sub> and -OH > -COOH > -CHO > -CH<sub>3</sub>. The ability of H<sub>2</sub>O to form hydrogen bonds with -COOH, -OH, -CHO, and -CH<sub>3</sub> is as follows: -COOH > -OH > -CHO > -CH<sub>3</sub>. This study provides a theoretical basis for the integrated use of hydraulic fracturing techniques and coalbed gas injection and replacement.

## 1. Introduction

Currently, the coal industry faced challenges related to the "carbon peaking and carbon neutrality" goals. It aimed to achieve "green, low-carbon emissions, and clean, efficient utilization" in line with the "dual-carbon" objectives [1]. The industry focused on promoting environmentally friendly coal mining practices and the utilization of coal resources with low carbon emissions to meet national energy security demands [2]. Extraction of coalbed methane, despite its abundant reserves, posed significant challenges, and the excessive release of CO<sub>2</sub> contributed significantly to the greenhouse effect. CO<sub>2</sub> emission control technologies focused on enhancing energy efficiency, promoting

low-carbon energy utilization, and implementing CO<sub>2</sub> capture and storage methods [3]. Petroleum or natural gas reservoirs, saline aquifers, and underutilized coal seams were common CO<sub>2</sub> storage options. Global coal seams alone had a storage potential of 89.1 trillion to 269.0 trillion cubic meters [4]. Geological storage proved effective in mitigating environmental issues caused by CO<sub>2</sub> emissions, and the displacement of CO<sub>2</sub> for coalbed methane recovery offered promising environmental and economic benefits.

Scholars have extensively conducted laboratory research on the adsorption characteristics of methane and carbon dioxide on coal. Moffat investigated the high-pressure adsorption of carbon dioxide in bituminous coal and revealed its occurrence in coal seams [5]. Wang

\* Corresponding author. College of Safety Science and Engineering (Henan Polytechnic University), Jiaozuo 454003, China.

E-mail addresses: [yhmfs@163.com](mailto:yhmfs@163.com) (H. Yang), [Kangnning@163.com](mailto:Kangnning@163.com) (N. Kang), [chenxj0517@126.com](mailto:chenxj0517@126.com) (X. Chen), [15735656024@163.com](mailto:15735656024@163.com) (Y. Liu).

conducted experiments using a custom coal sample adsorption apparatus to explore the impact of moisture, pH value, and coal metamorphism on carbon dioxide adsorption. They identified the conditions for enhancing CO<sub>2</sub> storage in coal seams [6]. Zhang focused on studying the influence of CO<sub>2</sub> exposure on the adsorption behavior of different coal types under high-pressure conditions. They proposed potential mechanisms for the dependence of coal adsorption performance on CO<sub>2</sub> exposure [7]. Previous studies primarily investigated the adsorption behavior of methane and carbon dioxide on coal under simulated reservoir conditions, demonstrating that carbon dioxide exhibits higher adsorption capacity and rate compared to methane [8–10]. Additionally, investigations into the injection of carbon dioxide into methane-saturated coal seams provided further evidence supporting the feasibility of methane recovery through carbon dioxide sequestration.

To achieve efficient implementation of CO<sub>2</sub>-ECBM, scholars have extensively investigated the microscopic interaction mechanisms between coal and CH<sub>4</sub>/CO<sub>2</sub> [11]. Fu utilized density functional theory (DFT-D3) to study the promotional effect of CO<sub>2</sub> adsorption on the desorption of CH<sub>4</sub> from low-rank coal macerals. It was elucidated that CO<sub>2</sub> adsorption facilitates CH<sub>4</sub> desorption, while CH<sub>4</sub> cannot displace CO<sub>2</sub> in coal [12]. Weinberger conducted comprehensive classical Monte Carlo simulations to determine the adsorption process of equimolar binary mixtures (O<sub>2</sub>–CO<sub>2</sub>, H<sub>2</sub>–CH<sub>4</sub>, and CH<sub>4</sub>–CO<sub>2</sub>) in porous materials [13]. Wang employed molecular simulations to investigate the adsorption and diffusion behaviors of CO<sub>2</sub> and CH<sub>4</sub> in coal seams, comparing their adsorption capacities and isotherms in single-component and binary mixtures and demonstrated a significant decrease in CH<sub>4</sub> adsorption capacity in binary mixtures due to the presence of CO<sub>2</sub> [14].

Both domestic and international scholars have conducted extensive physical experiments to study the adsorption characteristics of methane and carbon dioxide in coal [15–17]. However, most of these experiments focused on dry coal and did not consider the presence of water in coal seams, which can significantly influence gas adsorption. Consequently, many scholars have investigated the impact of water on gas adsorption and displacement in coal [8,18,19]. However, there is still uncertainty regarding how to ensure efficient adsorption of methane and carbon dioxide in the presence of water. Additionally, there is a limited number of studies that analyze the adsorption mechanism at the atomic and molecular levels. The comprehensive consideration of molecular mechanics, molecular dynamics, quantum mechanics, and other factors that influence intermolecular interactions is lacking, leading to an incomplete understanding of the dynamic processes involved in intermolecular interactions.

Coal is a highly complex organic polymer consisting of diverse functional groups and a mixture of aliphatic and aromatic compounds [11,20]. Distinct differences in adsorption affinities between CO<sub>2</sub> and CH<sub>4</sub> are observed when they interact with different functional groups. These differences arise from variations in their polarity, basicity, and acidity [21–23]. Investigations into the adsorption properties and the impact of functional groups on the adsorption selectivity of CO<sub>2</sub> and CH<sub>4</sub> are of significant interest in CBM and CCS engineering. Surface functionalization is the dominant factor that determines the gas adsorption mechanism in coals [21–24]. Liu conducted investigations into the effects of oxygen-containing surface functionalities on the adsorption of mixtures, including CO<sub>2</sub>/CH<sub>4</sub>, CO<sub>2</sub>/N<sub>2</sub>, and CO<sub>2</sub>/H<sub>2</sub>O. The study revealed that these oxygen-containing functionalized surfaces not only enhance the total adsorption of CO<sub>2</sub> but also improve the separation selectivity of specific gas mixtures [25,26]. Nevertheless, there remain numerous uncertainties regarding the effectiveness of oxygen-containing functional groups in CO<sub>2</sub>/CH<sub>4</sub> adsorption, as well as the underlying mechanisms.

This study utilized a combination of physical experiments and molecular simulations. Anthracite samples were obtained from the No. 15 seam of Shangshe No.2 well in Yangquan, Shanxi Province. Isothermal adsorption experiments of CH<sub>4</sub> and CO<sub>2</sub> were carried out on anthracite samples with varying moisture contents using the isobaric diffusion

method. Qualitative and quantitative analyses were conducted to investigate the effects of moisture interference on CH<sub>4</sub> and CO<sub>2</sub> adsorption by anthracite. This manuscript systematically investigates the impact of oxygen-containing functional groups (-OH, -COOH, -CHO) on the water inhibition of CO<sub>2</sub>/CH<sub>4</sub> adsorption characteristics and their underlying mechanisms. The investigation is based on a molecular model of anthracite coal (C<sub>202</sub>H<sub>104</sub>O<sub>21</sub>N<sub>2</sub>S<sub>2</sub>) using Materials Studio software. Initially, the geometry and energy of C<sub>202</sub>H<sub>104</sub>O<sub>21</sub>N<sub>2</sub>S<sub>2</sub> were optimized using molecular mechanics (MM) and molecular dynamics (MD) methods. Subsequently, the adsorption process of CO<sub>2</sub>/CH<sub>4</sub> under varying moisture conditions was examined. Additionally, the changes in intermolecular interaction energy, van der Waals energy, and electrostatic energy during the adsorption process were analyzed using GCMC and DFT-D3 methods. Oxygen-containing functional groups' effects on adsorption properties and the synergistic interactions among neighboring functional groups during CO<sub>2</sub>/CH<sub>4</sub> adsorption were simulated by substituting synergistic functional groups. This approach isolated the effects of the target groups while excluding other functional groups. Optimal adsorption configurations for various edge functionalized sites were then determined and described. Consequently, this study offers greater fidelity compared to prior research. It offers valuable insights into the modification of anthracite surfaces through the adsorption of oxygen-containing functional groups. Moreover, it carries significant implications for enhancing the separation and purification of CO<sub>2</sub>/CH<sub>4</sub> mixtures in CCUS and ECBM engineering.

## 2. Experimental plan

### 2.1. Experimental coal samples

The anthracites utilized in the experiments were obtained from No. 15 seam of Shangsha No. 2 well in Yangquan. The gangue-free lump coal, recently exposed at the working face, was sealed and transported back to the laboratory. The 60–80 mesh (0.18mm–0.25 mm) granular pulverized anthracite underwent sieving using a standard sieve. Subsequently, it was dried in an oven at a temperature of 105 °C for more than 10 h [27–29]. Following the aforementioned treatment, the anthracite was deemed to be completely devoid of moisture and served as blank controls. Subsequently, all the dried anthracite was removed and allowed to cool to room temperature before being set aside. Table 1 displays the results of the industrial analysis, along with the true relative density and apparent relative density of the anthracite.

This paper investigates the impact of moisture on the characteristics of coal adsorbed gas, specifically focusing on the moisture content within the original coal seam. Consequently, it is crucial to control the moisture gradient within a specific range. By consulting relevant data and considering the on-site conditions, we have established the moisture gradient for anthracite in this experiment, which includes the following levels: 0 %, 0.75 %, 1.5 %, 2.25 %, and 3 %. In addition, a separate control experiment was conducted using dry anthracite. The moisture content of the anthracite was determined using the moisture calculation Eq. (1) [18]. The results of the anthracite preparation are presented in Table 2.

$$Y = \frac{x}{x + 180} \times 100\% \quad (1)$$

Where Y is the moisture content of anthracite (%), x is moisture to be added (g).

### 2.2. Experimental system

This paper aims to investigate the isothermal adsorption characteristics of single-component CH<sub>4</sub> and CO<sub>2</sub> in anthracite with varying moisture contents. The physical experiment was conducted using a multi-element gas displacement device designed for gas-bearing coal. The device comprises five main components: a high-pressure gas supply

**Table 1**

True relative density, apparent relative density and industrial analysis results of the anthracite.

Indicators	Moisture (%)	Ash content (%)	Volatile fraction (%)	True relative density (g/cm <sup>3</sup> )	Apparent relative density(g/cm <sup>3</sup> )	Porosity (%)
Measured value	1.67	17.03	12.12	1.52	1.41	7.24

**Table 2**

Preparation of moisture-bearing anthracite.

Moisture content of anthracite/%	Mass of anthracite/g	Moisture addition/g
0.75	180	1.36
1.5	180	2.74
2.25	180	4.62
3	180	5.57

system, a constant temperature adsorption-desorption system, a gas composition analysis system, a vacuum system, and a data acquisition system. The schematic diagram of the experimental device is presented in Fig. 1.

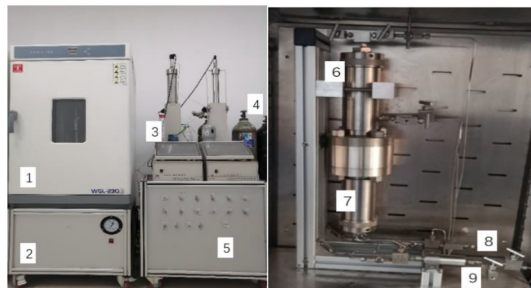
### 2.3. Experimental conditions

In this paper, the experimental conditions were designed using the control variable method. The adsorption equilibrium pressure, temperature, and moisture content were determined based on the actual occurrence characteristics of coal seam gas at the sampling point. These factors were calculated considering the coal seam burial depth, overlying strata bulk density, gas pressure, and humidity level at the sampling point, in conjunction with the principles of similarity theory. Following field measurements and theoretical calculations, the adsorption equilibrium pressures were set at 0.8 MPa, 1.2 MPa, 1.6 MPa, 2.0 MPa, and 2.4 MPa, respectively. The experimental temperature was maintained at 25 °C, and the moisture content was varied at 0 %, 0.75 %, 1.5 %, 2.25 %, and 3 %. A total of 10 sets of tests were conducted, involving five different coal samples. Each coal sample was subjected to separate CH<sub>4</sub> and CO<sub>2</sub> adsorption tests to assess their individual adsorption characteristics.

### 2.4. Experimental steps

- (1) The air tightness of the experimental device was tested.
- (2) The pressure test device underwent vacuum degassing.
- (3) The volume measurement of each pipeline in the pressure test device was conducted.
- (4) The determination of the residual volume of the coal sample chamber was performed. The residual volume refers to the true relative density value measured prior to placing the sample. The calculation formula as follows [15].

$$V_s = V_{ml} - V_c \quad (2)$$



1. Thermostat 2. Vacuum pump 3. Quantitative injection pump 4. Gas cylinder 5. Control valve 6. CO<sub>2</sub> injection tank 7. Coal sample tank 8. Air inlet valve 9. Vent valve

Fig. 1. Physical drawing of experimental platform.

$$V_c = \frac{G}{TRD_{20}} \quad (3)$$

Where  $V_s$  is residual volume of coal sample chamber (cm<sup>3</sup>),  $V_{ml}$  is volume of coal sample chamber (cm<sup>3</sup>),  $V_c$  is volume of pure coal sample (cm<sup>3</sup>),  $G$  is coal sample mass (g).  $TRD_{20}$  is true relative density of coal sample (g/cm<sup>3</sup>).

(5) In the gas adsorption equilibrium experiments, 180g of moisture-bearing anthracite was loaded into each of the three coal sample tanks. The experimental temperature was maintained at 25 °C, and the gas from the cylinder was introduced into the coal sample chamber for the adsorption test based on the predetermined adsorption pressure. When the pressure value error in the gas chamber reached 0.03 MPa, indicating that adsorption equilibrium was achieved, the corresponding adsorption equilibrium pressure was recorded. The experimental data for CH<sub>4</sub> and CO<sub>2</sub> adsorption were considered complete based on these recorded values. However, after each experiment, the entire pipeline needed to be vacuumized again to minimize errors caused by residual gas in subsequent experiments.

These steps were repeated to conduct isothermal adsorption experiments on five different moisture content anthracites, employing constant temperature and various adsorption equilibrium pressures. The isothermal adsorption curves for both gases were fitted using a multiple linear regression model, yielding the Langmuir fitting equation and curve for CH<sub>4</sub> and CO<sub>2</sub> gas adsorption in coal. By utilizing the Langmuir equation (Eq. (4)), the adsorption constants ( $a$  and  $b$ ) for both gases were calculated. Please note that the Langmuir equation (Eq. (4)) and the actual calculation of adsorption constants ( $a$  and  $b$ ) were not provided in the given information [30].

$$V = \frac{abP}{1 + bP} \quad (4)$$

Where  $P$  refers to the gas pressure at adsorption equilibrium (MPa). Through data processing, the values of  $a$  and  $b$  were calculated by fitting the Langmuir curve with  $P$  as the abscissa and  $V$  as the ordinate.

## 3. Simulation

### 3.1. Construction of molecular model

In this paper, the molecular structure of anthracite coal in the existing literature was screened and compared with the anthracite coal chosen for physical experiments. Finally, the molecular structure model of anthracite constructed by Cui was chosen for this paper, which can reasonably characterize the structural properties of anthracite [31]. The industrial and elemental analyses of the two anthracite coals are presented in Table 3. By analyzing the relative content of each element in anthracite, we calculated the ratios of various types of atoms in the molecular structure. These ratios significantly influence the differences in molecular structure, as illustrated in Table 4. Its molecular chemical formula is C<sub>202</sub>H<sub>104</sub>O<sub>21</sub>N<sub>2</sub>S<sub>2</sub>. Fig. 2 depicts the molecular structure model of anthracite.

Where Anthracite-1 represents the standard anthracite coal model GBW(E) 16110031, as utilized by Cui. Anthracite-2 refers to the anthracite coal sourced from Shangshe No.2 well in Yangquan, Shanxi Province. 'daf' denotes the dry ash-free basis, 'A<sub>d</sub>' represents ash

**Table 3**

Proximate analysis and Ultimate analysis of different anthracite coals.

Sample	Ultimate analisis, Wt%, daf					Proximate analysis, Wt%	
	C	H	O	N	S	Ad	V <sub>daf</sub>
Anthracite-1	81.4	3.51	11.12	1.16	2.81	8.68 %	10.8 %
Anthracite-2	82.6	3.32	10.8	1.23	2.70	17.03 %	12.12 %
Inaccuracy	1.47% %	9.11 %	6.83 %	6.03 %	6.76 %	49.03 %	9.25 %

**Table 4**

Atomic ratio of different anthracite coals.

Sample	H/C	O/C	N/C	S/C
Anthracite-1	0.517	0.102	0.012	0.013
Anthracite-2	0.482	0.098	0.013	0.012
Inaccuracy	6.71 %	3.86 %	6.36 %	5.71 %

content on a dry basis, and 'V<sub>daf</sub>' stands for the volatile fraction on a dry ashless basis.

In recognition of the significant interaction between anthracite

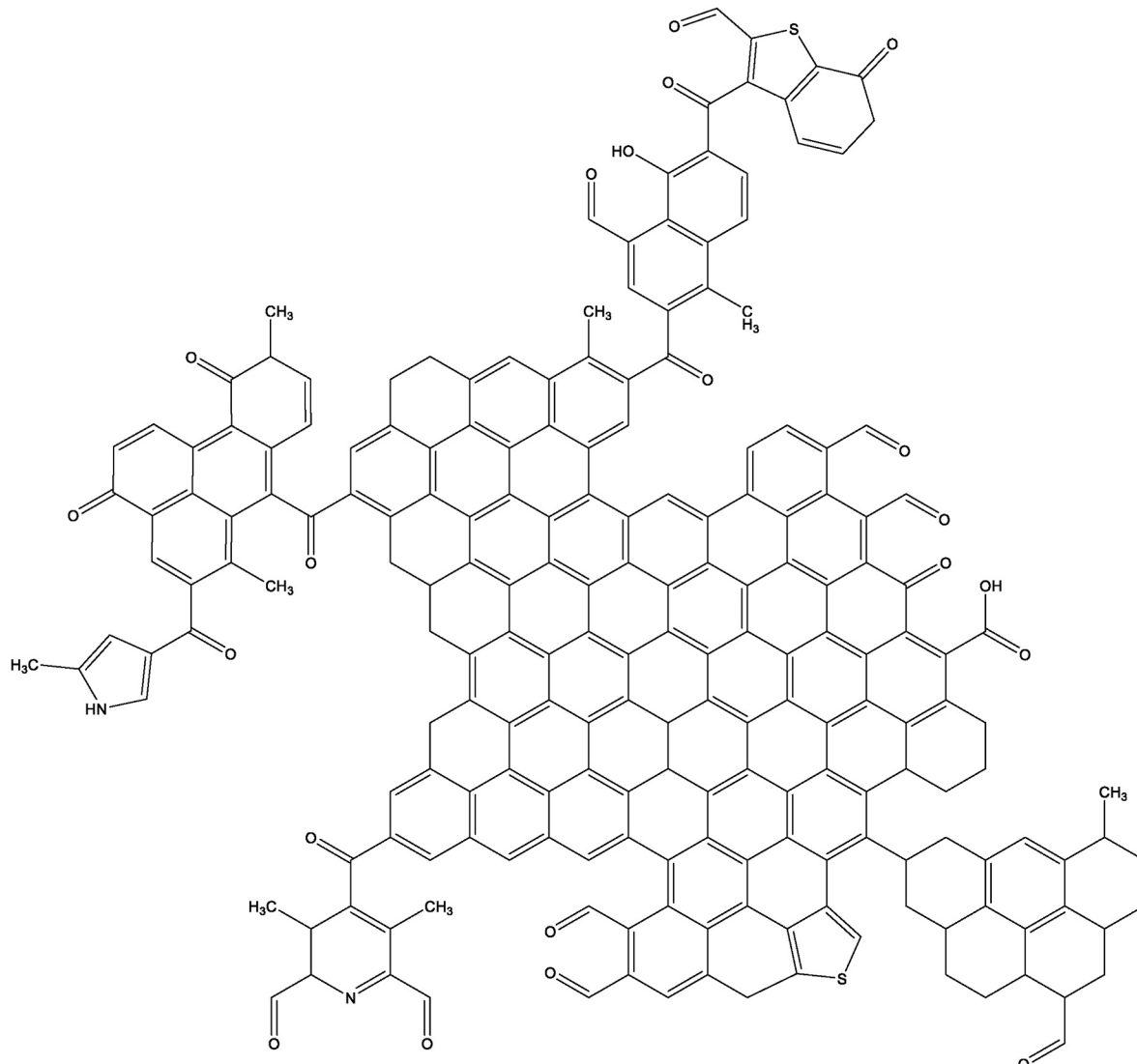
molecules, this paper focuses on a configuration system comprising four anthracite molecules (as depicted in Fig. 2) as the subject of investigation. To simulate the water concentration similar to that in the physical test, different quantities of H<sub>2</sub>O molecules were introduced (as specified in Table 5). Moisture content in molecular simulation was determined through the calculation of specific molecular weight. The count of water molecules could only be represented as an integer. Consequently, the moisture content in molecular simulation could only approximate that of physical experiments, but achieving an identical value was challenging. These additions allow for the determination of water concentration values that align with the conditions observed in the experimental setup approximately.

The moisture content of the anthracite in molecular simulations was

**Table 5**

Molecular structure of moisture-bearing anthracite.

Moisture content/%	Number of H <sub>2</sub> O molecules
0 %	0
0.76	5
1.5	10
2.23	15
2.95	20

**Fig. 2.** Two dimensional structure of anthracite molecules.

determined using Equation (5).

$$Y = \frac{m * n}{m * n + N * M} \times 100\% \quad (5)$$

Where Y represents the moisture content of anthracite, n signifies the number of water molecules within the system, N denotes the count of anthracite molecules within the system, m stands for the relative molecular mass of an individual water molecule, and M signifies the relative molecular mass of an individual anthracite molecule.

Following the specified quantities of  $\text{H}_2\text{O}$  molecules outlined in Table 5, the construction of the moisture-bearing anthracite configuration system was accomplished using the Materials Studio software, as depicted in Fig. 3.

In this paper, the influence of moisture on the adsorption of single component  $\text{CH}_4$  and  $\text{CO}_2$  on anthracite is studied, so the adsorbent is anthracite molecular structure.  $\text{H}_2\text{O}$ ,  $\text{CH}_4$  and  $\text{CO}_2$  are adsorbates [32]. The molecular structure models of  $\text{H}_2\text{O}$ ,  $\text{CH}_4$  and  $\text{CO}_2$  drawn by Materials Studio software are shown in Fig. 4.

### 3.2. Molecular dynamics simulation calculation

The COMPASS force field covers a wide range of covalent molecules, including common organic, inorganic small molecules and polymers. For these molecular systems, it has been parameterized to predict various properties of molecules in the separated and condensed phases. This force field is one of the most popular force fields at present. The COMPASS II force field is an upgraded version of COMPASS, offering broader coverage and greater universality [33].

For the calculation of dynamic properties in this study, the Force module of Materials Studio was utilized. The task selected was Dynamics, and the NVT canonical ensemble was employed. The initial velocities of the system followed the Boltzmann distribution. The simulation was conducted at a temperature of 298 K, with a total simulation time of 1 ns and a time step of 1.0 fs. The Nose method was used for temperature control, and the Ewald summation method was employed for van der Waals interactions. The truncation radius was set to 1.25 nm, and the accuracy level was set to Fine. To obtain the kinetic properties of the system, the trajectory file from 200 to 500 ps after

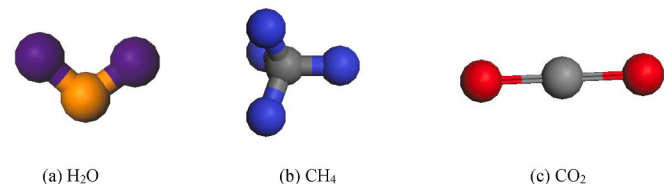


Fig. 4. Structural model of  $\text{H}_2\text{O}$  molecule,  $\text{CH}_4$  molecule and  $\text{CO}_2$  molecule.

achieving adsorption equilibrium was analyzed using Perl script.

The interaction energy is defined as the difference between the energy of a mixed system and the sum of the energies of each individual component in the system. It specifically quantifies the strength of intermolecular interactions and should not be confused with thermodynamic adsorption energy. The intermolecular interaction energy relationship allows us to analyze the strength of interactions between  $\text{H}_2\text{O}$ ,  $\text{CH}_4$ ,  $\text{CO}_2$ , and anthracite. The expression for the interaction energy between molecules in binary systems is represented by Eq. (6), while Eq. (7) represents the expression for the interaction energy between molecules in ternary systems [34,35].

$$E_{int(A-B)} = \frac{E_{total} - E_A - E_B}{2} \quad (6)$$

$$E_{int(A-B)} = \frac{E_{total} - E_B - E_{A+C} - E_A - E_{C+B} + E_C + E_{A+B}}{2} \quad (7)$$

Where A, B, and C represent three different molecules.  $E_{int}$  is the total interaction energy of the system (kJ/mol),  $E_{total}$  is the total energy of the system (kJ/mol).  $E_A$  is the energy of A in the system (kJ/mol),  $E_B$  is the energy of B in the system (kJ/mol),  $E_C$  is the energy of C in the system (kJ/mol).  $E_{A+B}$  represents the interaction energy between A and B in the system (kJ/mol).  $E_{A+C}$  denotes the interaction energy between A and C in the system (kJ/mol).  $E_{B+C}$  signifies the interaction energy between B and C in the system (kJ/mol).

Similarly, the van der Waals energy ( $E_{vdw}$ ) and electrostatic interaction energy ( $E_{elec}$ ) in the system can also be calculated using the formulas mentioned above. The corresponding calculation formulas are

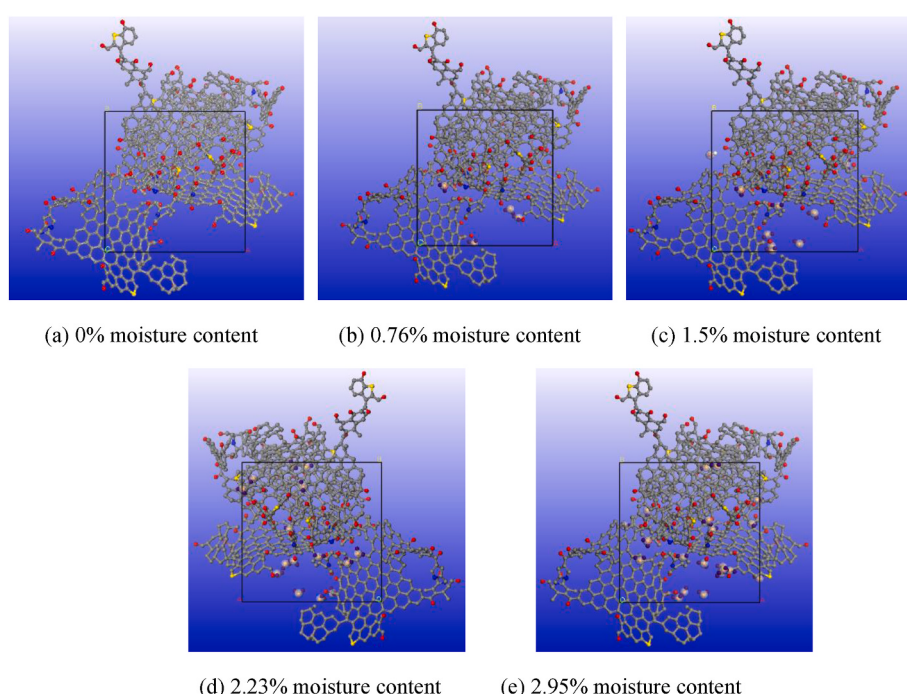


Fig. 3. Optimal molecular configuration of anthracite with different moisture content.

rewritten as Eq. (8) to Eq. (11).

$$E_{vdw(A-B)} = \frac{E'_{total} - E'_A - E'_B}{2} \quad (8)$$

$$E_{vdw(A-B)} = \frac{E'_{total} - E'_B - E'_{A+C} - E'_A - E'_{C+B} + E'_C + E'_{A+B}}{2} \quad (9)$$

$$E_{elec(A-B)} = \frac{E''_{total} - E''_A - E''_B}{2} \quad (10)$$

$$E_{elec(A-B)} = \frac{E''_{total} - E''_B - E''_{A+C} - E''_A - E''_{C+B} + E''_C + E''_{A+B}}{2} \quad (11)$$

Where A, B, and C represent three different molecules.  $E_{vdw}$  and  $E_{elec}$  are the total interaction van der Waals energy and the total interaction electrostatic energy of the system (kJ/mol).  $E'_{total}$  and  $E''_{total}$  are the total van der Waals energy and the total electrostatic energy of the system (kJ/mol).  $E'_A$  and  $E''_A$  are the van der Waals energy and the electrostatic energy of A in the system (kJ/mol).  $E'_B$  and  $E''_B$  are the van der Waals energy and the electrostatic energy of B in the system (kJ/mol).  $E'_C$  and  $E''_C$  are the van der Waals energy and the electrostatic energy of C in the system (kJ/mol).  $E'_{A+B}$  and  $E''_{A+B}$  are the van der Waals energy and the electrostatic energy between A and B in the system (kJ/mol).  $E'_{A+C}$  and  $E''_{A+C}$  are the van der Waals energy and the electrostatic energy between A and C in the system (kJ/mol).  $E'_{B+C}$  and  $E''_{B+C}$  the van der Waals energy and the electrostatic energy between B and C in the system (kJ/mol).

### 3.3. Monte Carlo simulation

In this paper, the adsorption isotherms of CH<sub>4</sub> and CO<sub>2</sub> in anthracite were calculated under the conditions of 25 °C, adsorption equilibrium pressures of 0.8 MPa, 1.2 MPa, 1.6 MPa, 2 MPa, and 2.4 MPa, and varying molecular configuration moisture contents of anthracite at 0 %, 0.76 %, 1.5 %, 2.23 %, and 2.95 %. These calculations were performed using the Grand Canonical Monte Carlo (GCMC) simulation method within the Sorption module of the Materials Studio software [36].

The GCMC simulation was carried out using the Fix pressure task item, with the Metropolis algorithm employed and a calculation accuracy set to Fine. The task item is Fix pressure, and Metropolis is selected, with a calculation accuracy controlled as Fine. The maximum loading steps and production steps were both 100000. The number of temperature cycles was 15. Final temperature was set to 298K. The algorithm adopts the Smart method. The convergence criteria for Energy and Force were set to 0.001 kcal/mol and 0.5 kcal/mol/Å. The maximum number of iterations was set to 500. It should be noted that the molecular model achieved convergence within this limit, as demonstrated in Fig. 5. The force field was selected as COMPASS II. The charge was use current. The Ewald and Atom based methods were used for electrostatic energy and van der Waals energy.

### 3.4. Quantum mechanical simulation calculation

Given the complex surface structure and high molecular weight of anthracite, which can pose higher computational demands and longer calculation times. Therefore, in order to investigate the stable configuration of H<sub>2</sub>O, CH<sub>4</sub> and CO<sub>2</sub> molecules adsorbed on the surface of anthracite, the oxygen containing functional group fragments of coal samples were extracted. Specifically, three oxygen-containing functional groups were selected: carboxyl (Benzene-COOH), hydroxyl (Benzene-OH), and carbonyl (Benzene-CHO). Additionally, a control group without oxygen, benzyl (Benzene CH<sub>3</sub>), was also investigated.

For optimizing the molecular structures of the four types of anthracite with different functional groups, the DMol<sup>3</sup> module within the Materials Studio software was utilized. The optimization was performed by opening the DMol<sup>3</sup> calculation dialog box and selecting Geometry Optimization as the task. The calculation accuracy was Medium. The B3LYP hybrid functional with dispersion correction was selected, and the nuclear processing method was set as DSPP [37]. The Atomic orbital basis group selected the double numerical orbital basis group and orbital polarization function (DNP). Electron spin was not restricted. The maximum subspace value was set to 10. The preprocessor was enabled to expedite the convergence rate. The hot occupation option was checked, and the smart value was set to 0.005 Ha. Subsequently, energy calculations were performed using the converged file. The task selected for this step was Energy, and Fine was chosen for intensive reading. On the properties tab, electron density and electrostatics were selected to calculate the molecular structures of the different functional groups of anthracite, as illustrated in Fig. 6.

To analyze the charge and charge density distribution of each atom, the charge analysis of the molecular structures of the different functional groups of anthracite was conducted using the Dmol<sup>3</sup> module. As shown in Fig. 7, it provides valuable information for studying charge transfer and changes in electrostatic potential.

The electrostatic potential (ESP) is a useful tool for predicting the locations of electrophilic and nucleophilic reactions on the van der Waals surface of a molecule. Electrophilic centers possess a positive charge and tend to interact with negatively charged centers on the surface of the electrostatic potential [38,39]. The electrostatic potential is a real-valued function defined for molecular systems. It is represented as follows.

$$V_{tot}(r) = \sum_A \frac{Z_A}{|r - R_A|} - \int \frac{\rho(r')}{|r - r'|} dr' \quad (12)$$

Where Z is the nuclear charge of atom A,  $R_A$  is the nucleus coordinate,  $\rho$  is the electron density function,  $r$  is the spatial coordinate, and  $r'$  is an arbitrary point on the atomic interface.

ESP is crucial for predicting intermolecular interactions, particularly non-covalent bonding interactions such as hydrogen bonding. Regions with high electrostatic potential values may function as hydrogen bond donors, whereas regions with low electrostatic potential values suggest potential hydrogen bond acceptors. Therefore, the electrostatic

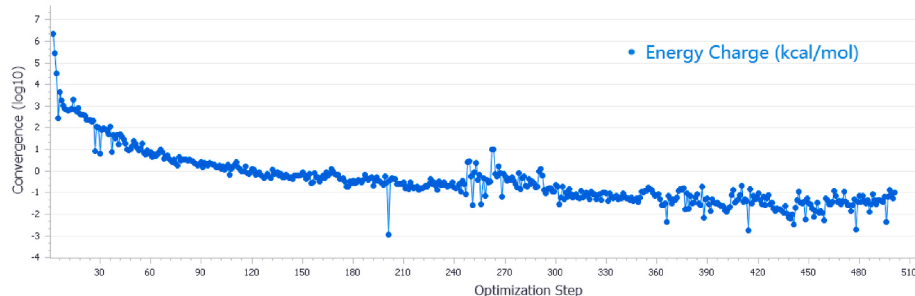
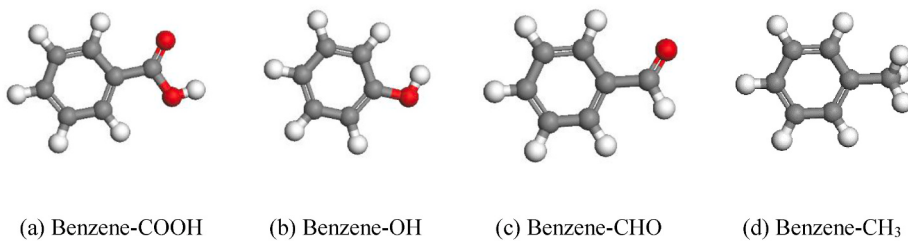
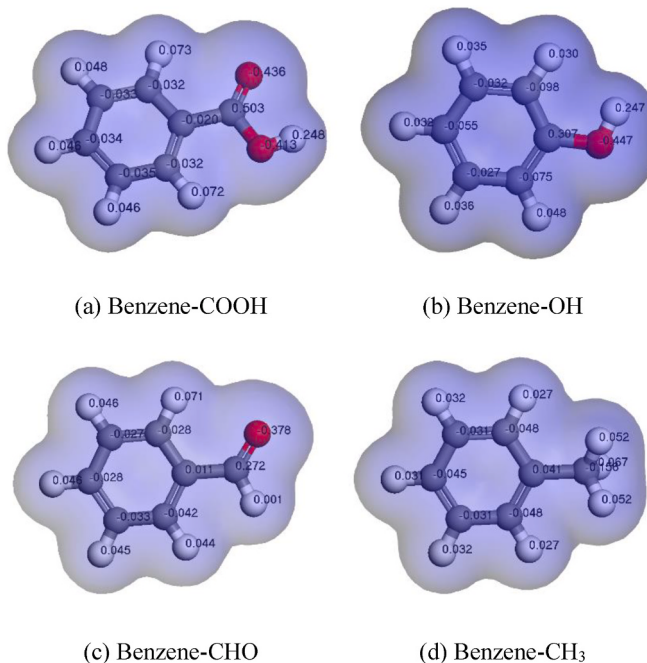


Fig. 5. Model convergence plot.

**Fig. 6.** Molecular structures of different functional groups of anthracite.**Fig. 7.** Charge density distribution of different oxygen-containing functional groups of anthracite.

potential plays an important role in the analysis of intermolecular interactions [40].

#### 4. Results and discussion

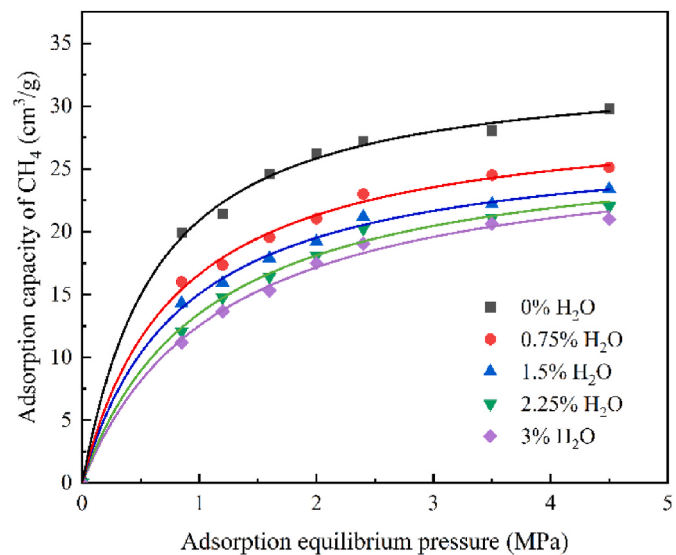
##### 4.1. Characteristics of the effect of moisture on the isothermal adsorption capacity of different gases

The isothermal adsorption experiments were conducted to investigate the adsorption of CH<sub>4</sub> and CO<sub>2</sub> by anthracite coal under various moisture contents. The experiments were performed at a constant temperature of 25 °C. The experimental results for the adsorption of CH<sub>4</sub> and

CO<sub>2</sub> by anthracite under different moisture contents were obtained and are presented in **Table 6**. The corresponding isothermal adsorption curves for CH<sub>4</sub> (**Fig. 8**) and CO<sub>2</sub> (**Fig. 9**) were plotted based on the data provided in **Table 6**.

**Table 4** clearly shows that the adsorption amount of CO<sub>2</sub> in anthracite is consistently higher than that of CH<sub>4</sub> under identical conditions, suggesting a preference for CO<sub>2</sub> adsorption. This study demonstrates a consistent pattern with the findings of Yves Gensterblum [41]. This can be primarily attributed to the following factors: (a) The gas adsorption capacity is generally proportional to the molecular weight of the adsorbent. CO<sub>2</sub> has a larger molecular weight compared to CH<sub>4</sub>, resulting in higher CO<sub>2</sub> adsorption amounts than CH<sub>4</sub>. (b) The gas adsorption amount is generally inversely proportional to the kinetic diameter of the adsorbent molecules. In comparison to CH<sub>4</sub> with a kinetic diameter of 0.38 nm, CO<sub>2</sub> has a smaller kinetic diameter of 0.33 nm.

According to the classification criteria proposed by the International

**Fig. 8.** Isothermal adsorption curve of CH<sub>4</sub>.**Table 6**

Experimental results of isothermal adsorption of CH<sub>4</sub>/CO<sub>2</sub> by coal with different moisture content.

Adsorption equilibrium pressure (MPa)	Adsorption amount (cm <sup>3</sup> /g)									
	0 %		0.75 %		1.5 %		2.25 %		3 %	
	CH <sub>4</sub>	CO <sub>2</sub>	CH <sub>4</sub>	CO <sub>2</sub>	CH <sub>4</sub>	CO <sub>2</sub>	CH <sub>4</sub>	CO <sub>2</sub>	CH <sub>4</sub>	CO <sub>2</sub>
0.85	19.92	31.24	16.02	30.22	14.33	25.33	12.07	20.21	11.19	17.60
1.2	21.43	33.98	17.37	31.87	15.94	26.77	14.78	21.92	13.65	19.23
1.6	24.58	35.76	19.54	33.9	17.88	30.71	16.42	24.81	15.33	22.01
2	26.25	37.23	21.03	35.48	19.23	32.97	18.09	28.17	17.49	25.67
2.4	27.23	38.24	23.00	37.28	21.2	33.8	20.23	29.71	19.02	26.76
3.5	28.04	39.56	24.51	38.01	22.21	34.63	21.1	30.02	20.63	27.67
4.5	29.78	40.39	25.11	38.99	23.4	35.41	22.01	30.92	21.01	28.11

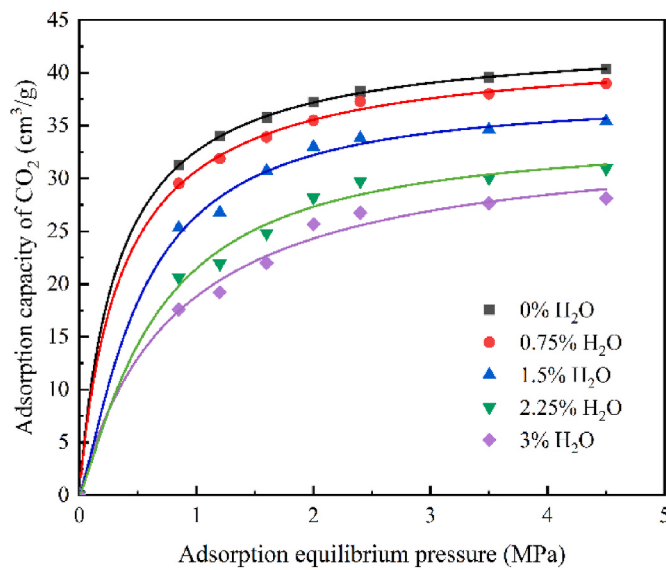


Fig. 9. Isothermal adsorption curve of CO<sub>2</sub>.

Union of Pure and Applied Chemistry (IUPAC) for physical adsorption isotherms, the isothermal adsorption curves of moisture-bearing anthracite exhibited characteristics consistent with the type I isotherm [42]. Therefore, the Langmuir single-layer adsorption model is suitable for describing the adsorption behavior of moisture-bearing anthracite for CH<sub>4</sub>/CO<sub>2</sub>. Figs. 8 and 9 demonstrate that the adsorption isotherms of CH<sub>4</sub>/CO<sub>2</sub> by anthracite follow a similar trend. As the adsorption equilibrium pressure increases, the adsorption amounts initially increase rapidly and then gradually level off [43].

Fig. 8 reveals that dry anthracite exhibits the highest adsorption capacity for CH<sub>4</sub>, and as the moisture content increases, the adsorption capacity for CH<sub>4</sub> gradually decreases. Previous studies consistently found that dry coal samples exhibited higher gas adsorption capacity than wet coal samples [12,23,24,40]. The maximum difference in adsorption is 9.25 cm<sup>3</sup>/g. Fig. 9 shows a significant decrease in CO<sub>2</sub> adsorption capacity in anthracite when the moisture content exceeds 1.5 %. With increasing moisture, the adsorption capacity of CO<sub>2</sub> decreases, with a maximum difference in adsorption of 13.64 cm<sup>3</sup>/g. It is evident that moisture significantly inhibits the adsorption of CH<sub>4</sub> and CO<sub>2</sub> by anthracite. This phenomenon can be attributed to the distribution of moisture within coal samples. In cases where the moisture mass fraction in coal is high, moisture is distributed across micropores, small pores, and medium-large pores. Conversely, when the moisture content is low, moisture predominantly exists within micropores. Consequently, the adsorption of CH<sub>4</sub>/CO<sub>2</sub> decreases with increasing moisture content, although the extent of CH<sub>4</sub>/CO<sub>2</sub> inhibition by moisture varies. When the moisture content increases from 0 to 1.5 %, moisture primarily occupies the micropores, resulting in a significant decrease in gas adsorption. However, as the moisture content increases from 1.5 % to 3 %, moisture begins to infiltrate the small and medium-large pores, leading to a relatively smaller reduction in gas adsorption. This phenomenon is a result of water presence within the coal pores, leading to capillary phenomena and the subsequent development of capillary resistance, which obstructs the passage of methane molecules into the microporous spaces. Since the inner specific surface area of micropores primarily facilitates gas adsorption in coal, the presence of capillary resistance makes it challenging for some micropores in coal to adsorb methane effectively. Consequently, the inhibitory effect of moisture on CH<sub>4</sub>/CO<sub>2</sub> adsorption primarily arises from its impact on gas adsorption within micropores.

According to the results of the adsorption of CH<sub>4</sub>/CO<sub>2</sub> by anthracite configuration calculated by Materials Studio software (Table 7), as shown in Fig. 10. The simulation results demonstrate that the anthracite

structure adsorbs CH<sub>4</sub>/CO<sub>2</sub>, which conforms to the Langmuir single-layer adsorption model. And the adsorption variation of CH<sub>4</sub>/CO<sub>2</sub> is consistent with the physical experiment results (Table 6, Figs. 8, Fig. 9). This further indicates the accuracy of the molecular structure of anthracite, CH<sub>4</sub>, CO<sub>2</sub> and H<sub>2</sub>O, and ensures the reliability of the subsequent simulation results.

Since the Langmuir model effectively describes the relationship between gas adsorption and moisture content, the adsorption constants of CH<sub>4</sub> and CO<sub>2</sub> can be determined using Langmuir fitting based on the results presented in Figs. 8 and 9. The results of the fitting calculations for the adsorption constants are presented in Table 8. Subsequently, the adsorption constants were further correlated with the moisture content, as depicted in Figs. 11 and 12.

The adsorption constant "a" represents the maximum adsorption capacity of coal [43]. Fig. 11 demonstrates that the value of "a" for CO<sub>2</sub> is higher than that for CH<sub>4</sub>, indicating that anthracite has a greater ultimate adsorption capacity for CO<sub>2</sub> compared to CH<sub>4</sub>. With increasing moisture content, the values of "a" for both CH<sub>4</sub> and CO<sub>2</sub> gradually decrease. Moisture clearly hinders the adsorption of CH<sub>4</sub> and CO<sub>2</sub> by coal. This phenomenon can be attributed to the stronger adsorption affinity of anthracite for H<sub>2</sub>O molecules compared to CH<sub>4</sub> and CO<sub>2</sub> when the moisture content is below 3 %. Consequently, H<sub>2</sub>O molecules compete with CH<sub>4</sub>/CO<sub>2</sub> molecules for adsorption, leading to a decrease in the gas adsorption capacity of anthracite. Additionally, Fig. 11 indicates a certain functional relationship between the adsorption constant "a" and the moisture content. For CH<sub>4</sub>, there is a linear relationship between "a" and the magnitude of the moisture content, which can be expressed as  $y = 43.447 - 3.348x$ . The fitting function has a coefficient of determination ( $R^2$ ) of 0.981, indicating a good fit. However, for CO<sub>2</sub>, the relationship is more accurately described by a power function. The functional relationship can be expressed as  $y = 29.114x^{(-0.063)}$ , and the fitting function has an  $R^2$  value of 0.956, indicating a good fit.

The adsorption constant "b" represents the rate at which coal adsorbs gases [44]. Fig. 12 illustrates that the adsorption rates of both CH<sub>4</sub> and CO<sub>2</sub> by coal gradually decrease with increasing moisture content, and the "b" value for CO<sub>2</sub> is higher than that for CH<sub>4</sub>. It shows that the adsorption rate of CO<sub>2</sub> by anthracite is much higher than that of CH<sub>4</sub>. As the moisture content increases, the adsorption rates of both CO<sub>2</sub> and CH<sub>4</sub> by anthracite become slower and approach each other. This can be attributed to the fact that H<sub>2</sub>O molecules occupy some of the adsorption sites in coal, thereby reducing the adsorption of gases by coal. The decrease in the "b" value for CO<sub>2</sub> suggests that the increase in moisture content has a greater impact on the adsorption rate of CO<sub>2</sub> compared to CH<sub>4</sub>. With increasing moisture content, the rate of CO<sub>2</sub> adsorption becomes slower. To accurately describe the relationship between the adsorption constant "b" and moisture content, the data were fitted in this study. The results indicate a linear relationship between the adsorption constant "b" and moisture content during the adsorption of methane by anthracite. The fitted relationship is expressed as  $y = 3.225 - 0.751x$ , with a good fit ( $R^2 = 0.961$ ). In the case of anthracite adsorption of carbon dioxide, the relationship between the two variables was better described by a polynomial equation with the expression  $y = 1.672 + 0.508x + 0.083x^2$ , resulting in a good fit ( $R^2 = 0.986$ ).

#### 4.2. Quantitative analysis of isothermal adsorption of water on different gases

The moisture influence coefficient is a crucial indicator for studying the impact of moisture on the variation of gas adsorption in coal. It quantifies the ratio of gas adsorption in a wet coal sample to that in a dry coal sample under identical conditions. Eq. (13) represents a commonly used linear functional equation [45].

$$\frac{V_m}{V_d} = \eta = \frac{1}{1 + a\omega} \quad (13)$$

**Table 7**Simulation results of isothermal adsorption of CH<sub>4</sub>/CO<sub>2</sub> by coal with different moisture content.

Adsorption equilibrium pressure (MPa)	Adsorption amount (n/u.c)									
	0 %		0.76 %		1.5 %		2.23 %		2.95 %	
	CH <sub>4</sub>	CO <sub>2</sub>	CH <sub>4</sub>	CO <sub>2</sub>	CH <sub>4</sub>	CO <sub>2</sub>	CH <sub>4</sub>	CO <sub>2</sub>	CH <sub>4</sub>	CO <sub>2</sub>
0	0	0	0	0	0	0	0	0	0	0
0.8	18.931	32.442	16.175	24.054	15.004	23.642	12.069	22.953	12.040	20.930
3.12	26.369	39.105	23.263	30.580	21.300	29.458	17.572	27.464	16.914	25.238
5.44	28.292	41.013	25.894	34.091	23.933	30.568	20.405	28.356	19.667	26.062
7.76	30.212	41.265	26.706	37.238	25.515	34.452	22.344	30.030	20.278	27.149
10.08	31.892	40.209	29.055	39.477	25.776	33.899	23.419	30.832	21.296	27.845
12.4	32.090	42.326	29.402	39.252	26.503	33.388	23.933	31.752	21.708	29.377
14.72	33.134	43.406	29.365	37.306	28.264	35.000	24.299	32.885	21.376	30.684
17.04	33.106	44.195	30.329	38.466	27.454	36.729	24.899	33.177	22.848	30.756
19.36	34.300	43.922	31.157	41.081	28.086	37.862	25.305	31.200	23.008	32.625
21.68	35.948	44.367	31.092	39.344	27.950	36.759	25.249	32.950	23.424	33.693
24.00	35.357	46.482	31.517	40.863	28.248	37.321	26.508	33.572	24.213	34.478

Where  $V_m$  is the adsorbed gas volume of wet coal under constant temperature gas pressure (cm<sup>3</sup>/g),  $V_d$  is the adsorbed gas volume of dry coal under constant temperature gas pressure (cm<sup>3</sup>/g),  $\eta$  is the moisture influence coefficient,  $a$  is the degree of influence of moisture content in coal sample and moisture influence coefficient.

In addition, a power function equation has been proposed as follows [46].

$$\frac{V_m}{V_d} = \eta = b\omega^{-c} \quad (14)$$

In this equation,  $b$  and  $c$  are constants.

Furthermore, an exponential functional equation is considered more suitable for characterizing the quantitative relationship between the moisture influence coefficient and moisture content [47].

$$\frac{V_m}{V_d} = \eta = \exp(-d\omega) \quad (15)$$

Where  $d$  represents the degree of influence of the moisture influence coefficient and moisture content.

Based on the data presented in Table 6, the adsorption amounts of CH<sub>4</sub> and CO<sub>2</sub> gases were determined for anthracite with varying moisture contents. To analyze the relationship between the moisture influence coefficient  $\eta$  and moisture content, the linear, exponential, and power function equations were fitted by incorporating Eq. (13)–(15). The results of this fitting were illustrated in Fig. 13.

Fig. 13(a) illustrates the fitted relationship between the moisture influence coefficient and moisture content during the adsorption of CH<sub>4</sub> by anthracite. The linear fit yields a correlation coefficient ( $R^2$ ) of 0.899, the power function fit has an  $R^2$  of 0.583, and the exponential fit results in an  $R^2$  of 0.909. Conversely, Fig. 13(b) displays the fitted relationship between the moisture influence coefficient and moisture content during the adsorption of CO<sub>2</sub> by different moisture-bearing anthracites. The linear fit has an  $R^2$  of 0.947, the power function fit shows an  $R^2$  of -19.002, and the exponential fit gives an  $R^2$  of 0.929.

It is evident that the power function fit has limitations or even inability to accurately represent the relationship between the moisture influence coefficient and moisture content for both CH<sub>4</sub> and CO<sub>2</sub> adsorption by anthracite. In contrast, the linear functional equation and exponential functional equation demonstrate better fitting accuracy. The exponential functional equation has a slightly higher  $R^2$  value than the linear functional equation when anthracite adsorbs CH<sub>4</sub>. Conversely, the exponential functional equation has a slightly lower  $R^2$  value than the linear functional equation when anthracite adsorbs CO<sub>2</sub>. Therefore, the exponential functional equation is relatively superior in describing the relationship between the moisture influence coefficient and moisture content during CH<sub>4</sub> adsorption, while the linear functional equation is better suited for CO<sub>2</sub> adsorption. Based on Fig. 13, it is evident that

moisture has a significant impact on the adsorption of CH<sub>4</sub> and CO<sub>2</sub> in anthracite, which aligns with the findings from Table 6 and Figs. 8 and 9.

#### 4.3. Interaction energy

The COMPASS II force field was employed to simulate the molecular system of anthracite with varying moisture content. The interaction energies between Anthracite-H<sub>2</sub>O, Anthracite-CH<sub>4</sub>, and Anthracite-CO<sub>2</sub> were calculated and analyzed using Perl script. By studying the change in interaction energy, the impact of moisture content on the adsorption of CH<sub>4</sub>/CO<sub>2</sub> in anthracite was examined. Specifically, we analyzed the changes in interaction energy during the equilibrium adsorption process of CH<sub>4</sub>/CO<sub>2</sub> in anthracite with varying moisture content at a pressure of 2.4 MPa. The results of this analysis are displayed in Figs. 14 and 15.

Figs. 14 and 15 provide insights into the energy composition during the adsorption process. The analysis reveals that the interaction energy is predominantly derived from van der Waals energy and electrostatic energy. The van der Waals energy constitutes a significant portion, accounting for approximately 80%–98% of the total interaction energy. It is worth noting that the interaction energy between anthracite and CH<sub>4</sub>/CO<sub>2</sub>/H<sub>2</sub>O is negative, indicating the spontaneous nature of the adsorption process. This signifies that anthracite exhibits an affinity for CH<sub>4</sub>, CO<sub>2</sub>, and H<sub>2</sub>O molecules.

In Fig. 14, the van der Waals energy between anthracite and CH<sub>4</sub> decreases from -132.622 kJ/mol to -373.283 kJ/mol, while the electrostatic energy decreases from -4.531 kJ/mol to -15.483 kJ/mol. Furthermore, the van der Waals energy between anthracite and H<sub>2</sub>O increases from -50.8375 kJ/mol to -15.5575 kJ/mol, and the electrostatic energy increases from -20.337 kJ/mol to -10.082 kJ/mol. As shown in Fig. 15, the van der Waals energy between anthracite and CO<sub>2</sub> decreases from -94.437 kJ/mol to -399.273 kJ/mol, and the electrostatic energy decreases from -15.026 kJ/mol to -48.383 kJ/mol. Additionally, the van der Waals energy between anthracite and H<sub>2</sub>O increases from -56.362 kJ/mol to -22.854 kJ/mol, and the electrostatic energy increases from -18.8925 kJ/mol to -9.7905 kJ/mol. Overall, the van der Waals interaction energy and electrostatic interaction energy between anthracite and CH<sub>4</sub>/CO<sub>2</sub> decrease with increasing moisture content. On the other hand, the van der Waals interaction energy and electrostatic interaction energy between anthracite and H<sub>2</sub>O increase as the moisture content increases. These results align with previous studies [35,48–51].

From the perspective of van der Waals energy, it can be observed that the force between H<sub>2</sub>O and anthracite is weaker compared to the force between anthracite and CH<sub>4</sub>/CO<sub>2</sub>. This indicates that the interaction strength between H<sub>2</sub>O and anthracite is relatively lower than the interaction strength between anthracite and CH<sub>4</sub>/CO<sub>2</sub>. Indeed, in addition to van der Waals forces, the presence of hydrogen bonding between anthracite and H<sub>2</sub>O plays a significant role. Hydrogen bonds are stronger

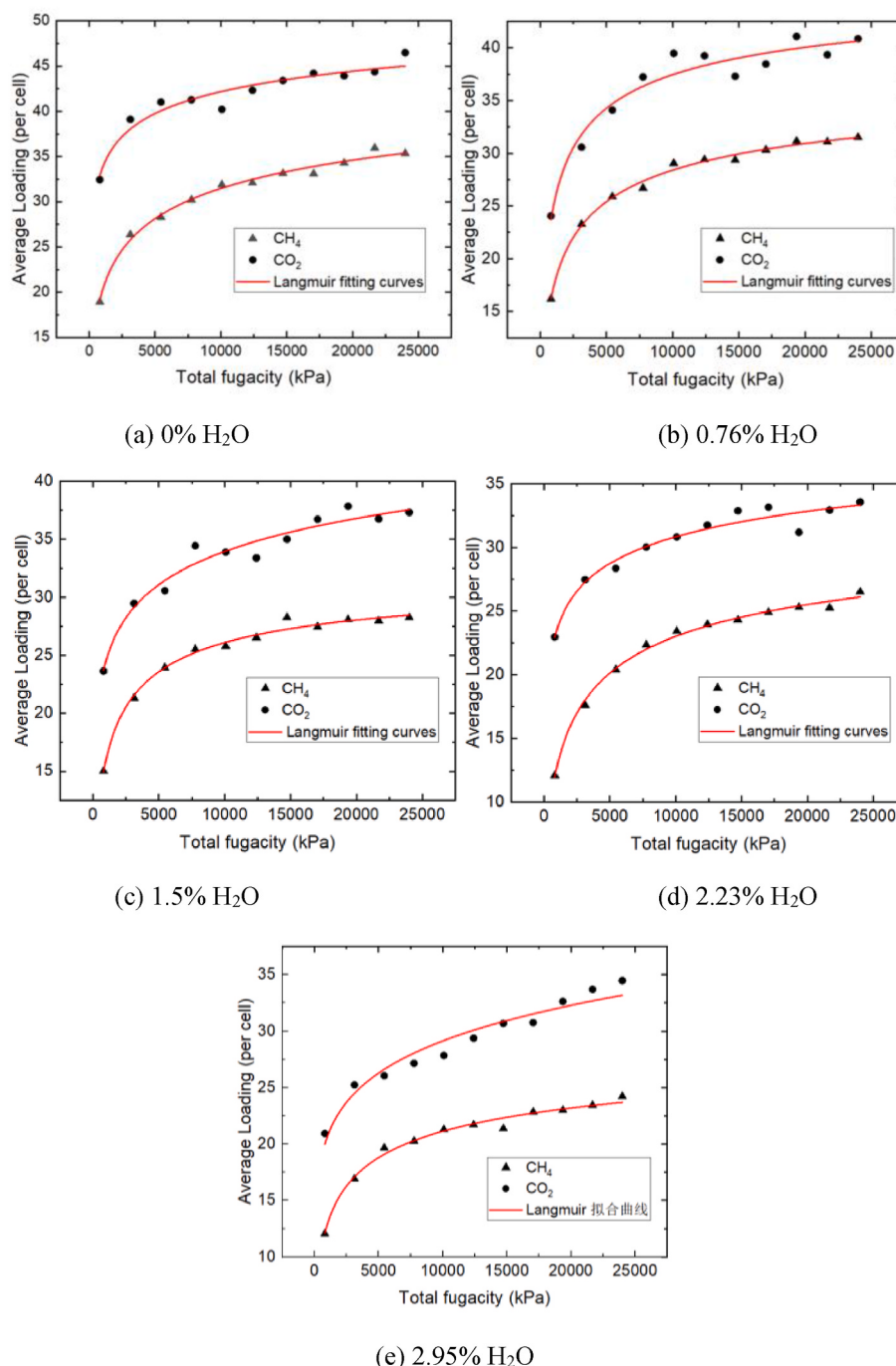


**Fig. 10.** Molecular simulation results of isothermal adsorption curve.

**Table 8**

Experimental results on the variation of adsorption constants a/b for CH<sub>4</sub>/CO<sub>2</sub> adsorption by coal with different moisture content.

Moisture content	Adsorption constant "a" (ml/g)		Adsorption constant "b" (MPa <sup>-1</sup> )	
	CH <sub>4</sub>	CO <sub>2</sub>	CH <sub>4</sub>	CO <sub>2</sub>
0 %	33.646	43.392	1.643	3.012
0.75 %	29.606	41.907	1.279	2.79
1.5 %	27.912	39.941	1.152	1.933
2.25 %	27.393	36.545	0.944	1.393
3 %	27.207	34.437	0.852	1.155

and more directional compared to van der Waals forces. Therefore, the force between anthracite and H<sub>2</sub>O is generally stronger than the force between anthracite and CH<sub>4</sub>/CO<sub>2</sub>. This indicates that water molecules have a competitive advantage and tend to occupy the effective adsorption sites on the surface of anthracite due to the presence of hydrogen bonding interactions.

#### 4.4. Adsorption characteristics of oxygen-containing functional groups

**Fig. 16** illustrates the van der Waals surface electrostatic potential projection of each oxygen-containing functional group. The red areas represent regions with positive electrostatic potential, with darker shades indicating higher electrostatic potential values. Conversely, the

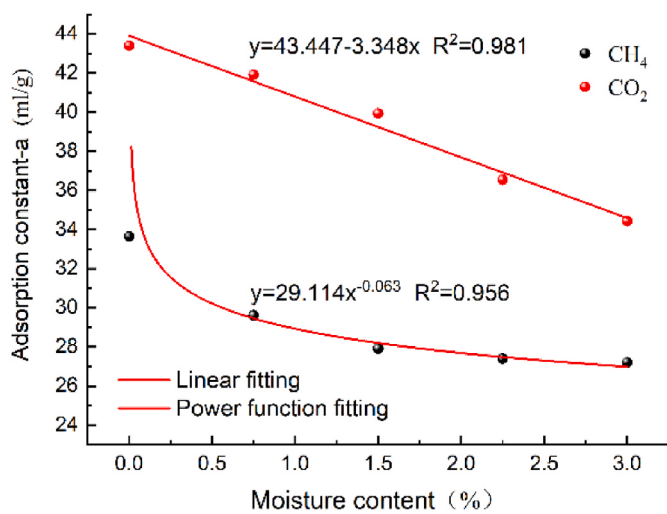


Fig. 11. Comparison of adsorption constant "a".

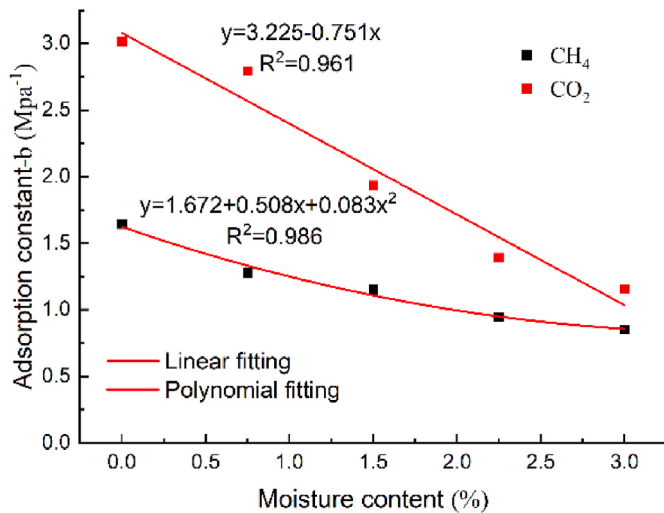


Fig. 12. Comparison of adsorption constant "b".

blue areas indicate regions with negative electrostatic potential, with darker shades indicating lower electrostatic potential values [51]. It can be observed that in Fig. 16, the oxygen atom in each oxygen-containing functional group generates ESP minimum points, indicated by the

presence of lone pair electrons. These ESP minimum points have relatively small electrostatic potential values.

From Fig. 16, it is evident that the ESP values near -COOH and -OH are relatively large compared to -CHO. Additionally, the maximum ESP values are located near the H atom. On the other hand, the ESP value near -CH<sub>3</sub> is the smallest. These observations can be attributed to the electronegativity of the O atom connected to the H atom, which leads to a strong positive charge on the H atom. As a result, this region becomes a favorable hydrogen bond donor due to the presence of the strong positive charge.

Based on the distribution characteristics of electrostatic potential in oxygen-containing functional groups, this study investigated the impact of H<sub>2</sub>O on the adsorption of CH<sub>4</sub>/CO<sub>2</sub> by different functional groups. The adsorption equilibrium conformations of CO<sub>2</sub>/CH<sub>4</sub> on moisture-bearing anthracite were depicted in Figs. 17 and 18. In these figures, the distances between CO<sub>2</sub>/CH<sub>4</sub> and oxygen-containing functional groups were measured from the center of the C atom to the O atom of the functional group. Similarly, the distances between CO<sub>2</sub>/CH<sub>4</sub> and benzyl was determined by measuring the length from the center of the C atom to the methyl C atom. On the other hand, the distances between H<sub>2</sub>O and oxygen-containing functional groups was calculated as the distances between the O atom and the O atom of the functional group. For benzyl, the distances were measured from the center between the O atom and the methyl C atom.

Based on Figs. 17 and 18, the adsorption sites of CH<sub>4</sub>, CO<sub>2</sub>, and H<sub>2</sub>O are primarily located near the -COOH, -OH, and -CHO functional groups. For the -CH<sub>3</sub> functional group, the adsorption sites are mainly concentrated near the benzene ring. The distances between CH<sub>4</sub> and the -COOH, -OH, -CHO, and -CH<sub>3</sub> groups range from 3.661 Å to 3.624 Å, 3.970 Å to 4.225 Å, 3.766 Å to 3.885 Å, and 3.769 Å to 4.269 Å, respectively. The distances between CO<sub>2</sub> and the -COOH, -OH, -CHO, and -CH<sub>3</sub> groups range from 3.823 Å to 4.211 Å, 3.877 Å to 4.357 Å, 4.076 Å to 5.907 Å, and 4.202 Å to 7.172 Å, respectively. The distances between H<sub>2</sub>O and the functional groups range from 2.882 Å to 4.332 Å. Typically, the range of van der Waals forces falls within 3 Å to 5 Å, suggesting that the adsorption of CH<sub>4</sub>/CO<sub>2</sub>/H<sub>2</sub>O and the functional groups primarily entails physical interactions between molecules [12, 52].

In addition to the van der Waals force, the presence of hydrogen bonds in the system was also considered. The distances between the H atom of methane and the O atom of the oxygen-containing functional group, the distance between the H atom of CH<sub>4</sub> and the O atom of the oxygen-containing functional group, the distance between the O atom of CO<sub>2</sub> and the H atom of the oxygen-containing functional group, the distance between the O atom of H<sub>2</sub>O and the H atom of the oxygen-containing functional group, and the distance between the H atom of H<sub>2</sub>O and the O atom of the oxygen-containing functional group were

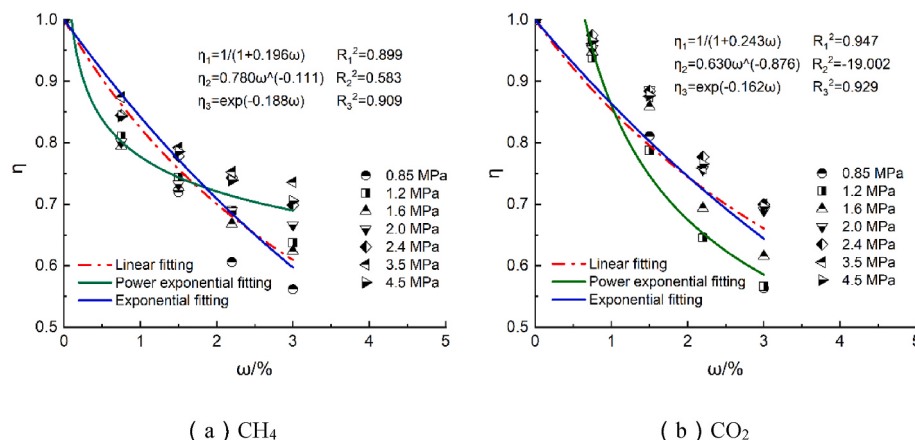
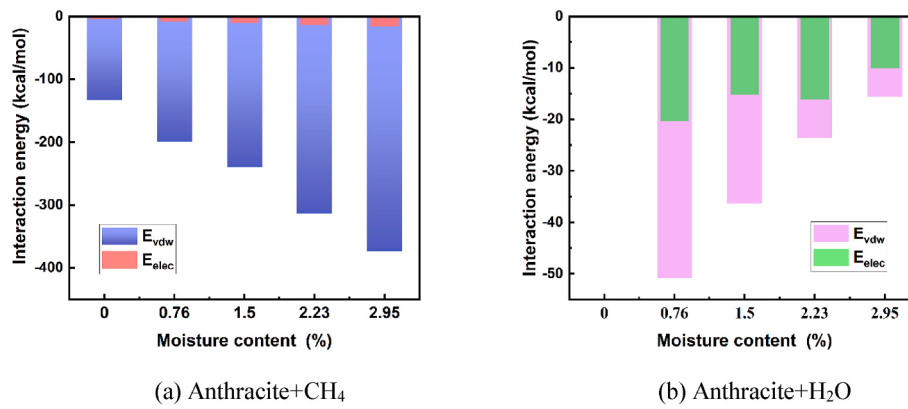
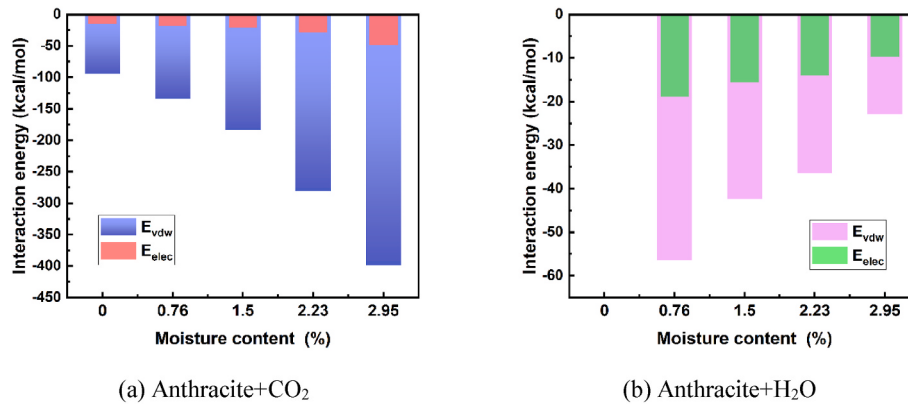


Fig. 13. Linear, exponential and power functions were used to fit the relationship between moisture influence coefficient and moisture content.



**Fig. 14.** The change diagram of the interaction energy between the molecules when the moisture-bearing anthracite adsorbs  $\text{CH}_4$ .



**Fig. 15.** The change diagram of the interaction energy between the molecules when the moisture-bearing anthracite adsorbs  $\text{CO}_2$ .

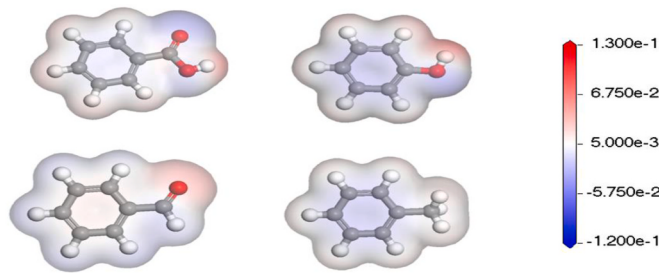


**Fig. 16.** The Van der Waals surface electrostatic potential diagram of oxygen-containing functional groups.

measured to assess the influence of hydrogen bonding. According to Fig. 17, in the presence of  $\text{H}_2\text{O}$ , when  $\text{CH}_4$  and Benzene-COOH combine, the distance between H and O atom increases from  $3.283 \text{ \AA}$  to  $3.289 \text{ \AA}$ . When  $\text{CH}_4$  binds to Benzene-OH, the distance between H atom and O atom increases from  $3.469 \text{ \AA}$  to  $3.725 \text{ \AA}$ . When  $\text{CH}_4$  binds to Benzene-CHO, the distance between H atom and O atom increases from  $3.262 \text{ \AA}$  to  $3.516 \text{ \AA}$ . When  $\text{CH}_4$  and Benzene-CH<sub>3</sub> combine, the distance between C atom and C atom decreases from  $4.269 \text{ \AA}$  to  $3.769 \text{ \AA}$ . According to the optimal adsorption conformation distance, the order of the binding capacity of  $\text{CH}_4$  to functional groups was Benzene-CHO > Benzene-COOH > Benzene-OH > Benzene-CH<sub>3</sub>. According to Fig. 18, the formation of hydrogen bonds between  $\text{CO}_2$  and oxygen-containing functional groups was mainly achieved through the combination of the O atom of  $\text{CO}_2$  with the H atom of the oxygen-containing functional group. According to Fig. 16, in the presence of  $\text{H}_2\text{O}$ , when  $\text{CO}_2$  and Benzene-COOH combine, the distance between O atom and H atom

increases from  $1.878 \text{ \AA}$  to  $4.328 \text{ \AA}$ . When  $\text{CO}_2$  and Benzene-OH combine, the distance between O atom and H atom increases from  $1.830 \text{ \AA}$  to  $4.160 \text{ \AA}$ . When  $\text{CO}_2$  combines with Benzene-CHO, the distance between O atom and H atom increases from  $4.964 \text{ \AA}$  to  $6.400 \text{ \AA}$ . When  $\text{CO}_2$  combines with Benzene-CH<sub>3</sub>, the distance between O atom and C atom increases from  $4.132 \text{ \AA}$  to  $7.872 \text{ \AA}$ . The order of the binding capacity of  $\text{CO}_2$  with functional groups can be determined as Benzene-OH > Benzene-COOH > Benzene-CHO > Benzene-CH<sub>3</sub>. Moreover, the insertion of  $\text{H}_2\text{O}$  increases the distances between  $\text{CH}_4$ ,  $\text{CO}_2$ , and the oxygen-containing functional group atoms, resulting in a weakening of the ability to form hydrogen bonds. This hinders the adsorption of  $\text{CH}_4$  and  $\text{CO}_2$  on anthracite.

Existing literature has demonstrated that surface oxygen functional groups with slightly higher hydrophobicity exhibit superior  $\text{CH}_4/\text{CO}_2$  adsorption capacity compared to less hydrophobic surface oxygen functional groups [53,54]. The reason for this phenomenon is that the functional groups -CHO, -COOH, and -OH are water-soluble and fall under the category of hydrophilic groups. Among these three groups, their hydrophilicity follows the order of -OH > -COOH > -CHO. Conversely, -CH<sub>3</sub> is insoluble in water and displays hydrophobic properties. Hence, in the presence of water, it becomes easier for water molecules to associate with oxygen-containing functional groups, leading to an increase in the distance between  $\text{CH}_4/\text{CO}_2$  and oxygen-containing functional groups. It becomes more challenging to establish van der Waals force interactions, thereby impeding the adsorption of coal and  $\text{CH}_4/\text{CO}_2$ . The methane binding affinity to oxygen-containing functional groups is observed in the order of Benzene-CHO > Benzene-COOH > Benzene-OH, while the carbon dioxide binding affinity to oxygen-containing functional groups follows the sequence of Benzene-OH > Benzene-COOH > Benzene-CHO. The

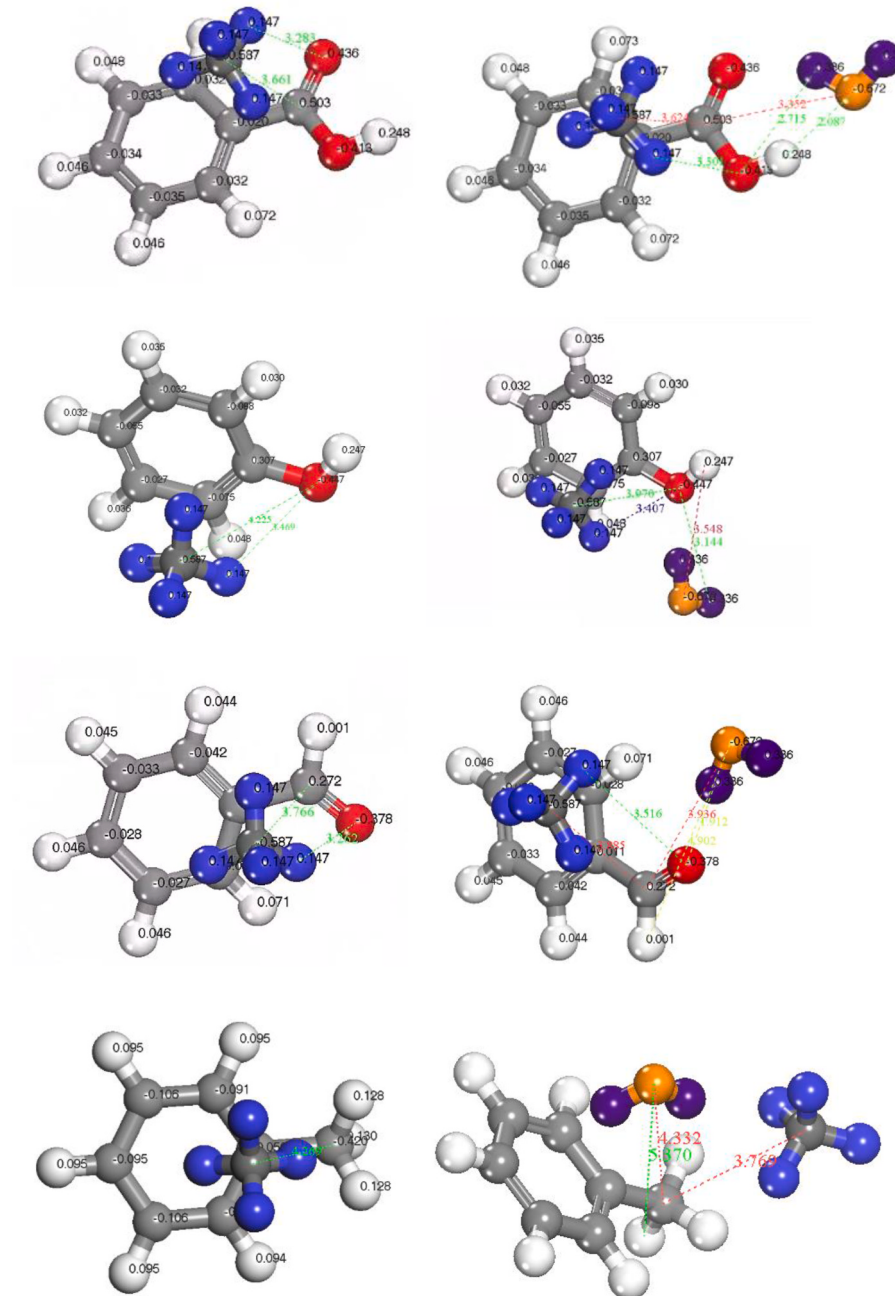


**Fig. 17.** The optimal molecular configuration diagram for the adsorption of  $\text{CH}_4$  by different oxygen-containing functional groups in the presence of moisture.

aforementioned disparity arises from the fundamental differences in the molecular properties of methane and carbon dioxide. When methane interacts with  $-\text{OH}$ ,  $-\text{COOH}$ ,  $-\text{CHO}$ , and  $-\text{CH}_3$  oxygen-containing functional groups, the water molecule's affinity for these oxygen-containing functional groups follows the order of Benzene-COOH > Benzene-OH > Benzene-CHO. Consequently, methane's binding capability to oxygen-containing functional groups exhibits the reverse order. On the other hand, carbon dioxide is a typical acidic gas. When it interacts with  $-\text{OH}$ ,  $-\text{COOH}$ ,  $-\text{CHO}$ , and  $-\text{CH}_3$  oxygen-containing functional groups, it prefers to associate primarily with the basic  $-\text{OH}$  group. Both  $-\text{COOH}$  and  $-\text{CHO}$  groups possess characteristics of acidity and basicity, but the hydroxide bond in the carboxyl group is more readily disrupted compared to that in  $-\text{CHO}$ , making  $-\text{COOH}$  more prone to binding with carbon dioxide. This preferential adsorption selectivity remains unchanged even in the presence of water.

According to Figs. 17 and 18, hydrogen bonds were indeed formed

between  $\text{H}_2\text{O}$  and oxygen-containing functional groups. There were two types of hydrogen bonds: the combination of the O atom of  $\text{H}_2\text{O}$  with the H atom of the oxygen-containing functional groups, and the combination of the H atom of  $\text{H}_2\text{O}$  with the O atom of the oxygen-containing functional groups [55].

In the case of Benzene-COOH,  $\text{H}_2\text{O}$  functions as a hydrogen bond donor. The distance between the O atom and the H atom measures 2.715 Å when  $\text{H}_2\text{O}$  binds to Benzene-COOH. Conversely, when  $\text{H}_2\text{O}$  acts as a hydrogen bond acceptor, the distance between the H atom and the O atom is 2.087 Å. For the  $-\text{COOH}$  functional group, water serves as a hydrogen bond acceptor, enhancing its propensity for hydrogen bonding. In the case of Benzene-OH, the lone pair of electrons on the oxygen in the hydroxyl group interacts with the hydrogen atoms in the water molecule, leading to the formation of a hydrogen bond. Hence, when  $\text{H}_2\text{O}$  can only function as a hydrogen bond donor, the distance between the H atom and the O atom of  $-\text{OH}$  is 3.584 Å. In the case of

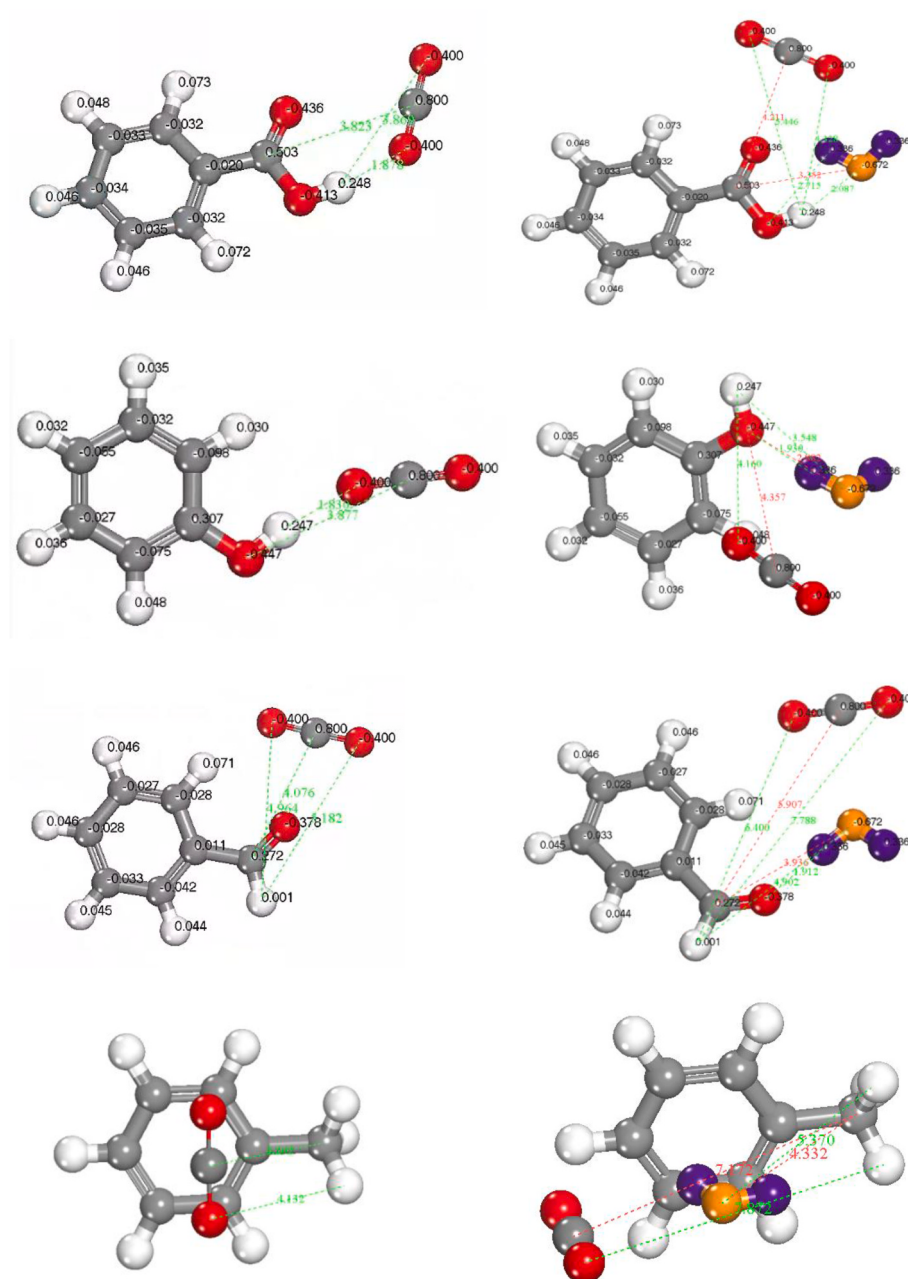


**Fig. 18.** The optimal molecular configuration diagram for  $\text{CO}_2$  adsorption by different oxygen-containing functional groups in the presence of moisture.

Benzene- $\text{CHO}$ , the H atom of  $-\text{CHO}$  is not directly connected to the O atom, and the electron cloud remains unshifted. Conversely, for Benzene- $\text{CH}_3$ ,  $\text{H}_2\text{O}$  can only serve as a hydrogen bond acceptor, resulting in a distance of 5.370 Å between the H and O atoms. Therefore, based on the interatomic distances observed during hydrogen bond formation,  $\text{H}_2\text{O}$  demonstrates the ability to form hydrogen bonds with  $-\text{COOH}$ ,  $-\text{OH}$ ,  $-\text{CHO}$ , and  $-\text{CH}_3$  in the following order:  $-\text{COOH} > -\text{OH} > -\text{CHO} > -\text{CH}_3$ . This aligns with the prevailing consensus that the moisture content of coal is intricately linked to the type and quantity of hydrophilic and hydrophobic functional groups present on its surface.

Prior research has established that water, in its adsorbed state, primarily forms hydrogen bonds with oxygen-containing functional groups on the coal surface and predominantly adheres to hydrophilic functional groups such as  $-\text{OH}$ ,  $-\text{COOH}$ ,  $-\text{C}\equiv\text{O}$ ,  $-\text{CHO}$ , and other similar groups [41,53,56,57]. These functional groups can serve as primary adsorption sites for  $\text{H}_2\text{O}$  molecules. This insight offers a novel approach for the effective implementation of hydraulic measures aimed at enhancing the

hydrophilicity of coal. By altering the nature of functional groups on the coal surface, it becomes possible to improve the efficiency of water injection into coal seams.

## 5. Conclusions

- Based on the analysis of the isothermal adsorption data for  $\text{CH}_4/\text{CO}_2$  under varying moisture conditions, it can be concluded that the adsorption constants ( $a$  and  $b$ ) for  $\text{CH}_4/\text{CO}_2$  decrease as moisture content increases. The patterns observed are as follows: for  $\text{CH}_4$  adsorption,  $y = 43.447 - 3.348x$  ( $a$ -value) and  $y = 3.225 - 0.751x$  ( $b$ -value); for  $\text{CO}_2$  adsorption,  $y = 29.114x - 0.063$  ( $a$ -value) and  $y = 1.672 + 0.508x + 0.083x^2$  ( $b$ -value).
- In the case of  $\text{CH}_4$  adsorption by coal, the exponential functional equation  $\eta = \exp(-0.188w)$  offers a better representation of the moisture influence coefficient. For  $\text{CO}_2$  adsorption by coal, the

- functional equation  $\eta = 1/(1 + 0.243\omega)$  provides a more accurate characterization.
- c. Through calculations and analysis of the interaction energy between molecules, it was observed that the interaction energy between coal and  $\text{CH}_4/\text{CO}_2/\text{H}_2\text{O}$  is negative, indicating the spontaneous adsorption of  $\text{CH}_4/\text{CO}_2/\text{H}_2\text{O}$  by coal. Furthermore, the van der Waals and electrostatic energies between coal and  $\text{CH}_4/\text{CO}_2$  decrease with increasing moisture content, whereas the van der Waals and electrostatic energies between coal and  $\text{H}_2\text{O}$  increase.
- d. The adsorption sites for  $\text{CH}_4/\text{CO}_2/\text{H}_2\text{O}$  are predominantly situated in proximity to the oxygen-containing functional groups. In the case of  $-\text{CH}_3$ , the adsorption sites are primarily concentrated near the benzene ring. The hydrogen bonding effect in the system mainly arises from the capability of  $\text{CH}_4/\text{CO}_2/\text{H}_2\text{O}$  to form hydrogen bonds with the functional groups. The hierarchy of hydrogen bonding ability between  $\text{CH}_4$  and functional groups is as follows:  $-\text{COOH} > -\text{OH} > -\text{CHO} > -\text{CH}_3$ . Similarly, for  $\text{CO}_2$ , the order of hydrogen bonding ability with functional groups is:  $-\text{OH} > -\text{COOH} > -\text{CHO} > -\text{CH}_3$ . In the case of Benzene-COOH,  $\text{H}_2\text{O}$  can function both as a hydrogen bond donor and acceptor. For Benzene-OH,  $\text{H}_2\text{O}$  can only act as a hydrogen bond donor, while for Benzene-COH and Benzene- $\text{CH}_3$ ,  $\text{H}_2\text{O}$  can solely serve as a hydrogen bond acceptor. The ability of  $\text{H}_2\text{O}$  to form hydrogen bonds with  $-\text{COOH}$ ,  $-\text{OH}$ ,  $-\text{CHO}$ , and  $-\text{CH}_3$  follows this order:  $-\text{COOH} > -\text{OH} > -\text{CHO} > -\text{CH}_3$ . These findings offer novel insights into modifying coal's properties to enhance its hydrophilicity and improve the efficient utilization of hydronization measures.

#### Credit author statement

1Hongmin Yang (First author): Funding acquisition; Data interpretation; Writing-review and editing  
 2Ningning Kang: Conceptualization; Methodology; Writing-manuscript draft; Data collection; Software; Graphing  
 3Xiangjun Chen (Corresponding author): Funding acquisition; Data interpretation; Writing-review and editing  
 4Yuan Liu: Writing-review and editing; Data collection

#### Notes

The authors declare no competing financial interest.

#### Declaration of competing interest

The authors declare that they have no known competing financial interests or personal relationships that could have appeared to influence the work reported in this paper.

#### Data availability

Data will be made available on request.

#### Acknowledgments

This research was supported by the National Natural Science Foundation of China (No. 52074105, No. 52074104, No. 52374195), the Key R & D and Extension Projects of Henan Province (No. 202102310223).

#### References

- [1] Yang P, Peng S, Benani N, Dong L, Li X, Liu R, Mao G. An integrated evaluation on China's provincial carbon peak and carbon neutrality. *J Clean Prod* 2022;377:134497.
- [2] Khattak SI, Ahmad M. The cyclical impact of innovation in green and sustainable technologies on carbon dioxide emissions in OECD economies. *Environ Sci Pollut Res* 2022;29(22):33809–25.
- [3] Zhi K, Li Z, Wang B, Klemeš JJ, Guo L. A review of  $\text{CO}_2$  utilization and emissions reduction: from the perspective of the chemical engineering. *Process Saf Environ Protect* 2023;172:681–99.
- [4] Liu S, Liu T, Zheng S, Wang R, Sang S. Evaluation of carbon dioxide geological sequestration potential in coal mining area. *Int J Greenh Gas Control* 2023;122:103814.
- [5] Moffat DH, Weale KE. Sorption by coal of methane at high pressure. *Fuel* 1995;34.
- [6] Wang X, Deng C, Qiao L, Chu G, Jing R, Kang Y. A study on factors influencing  $\text{CO}_2$  adsorption by coal. *AIP Adv* 2021;11(3):035238.
- [7] Zhang DF, Cui YJ, Liu B, Li SG, Song WL, Lin WG. Supercritical pure methane and  $\text{CO}_2$  adsorption on various rank coals of China: experiments and modeling. *Energy Fuels* 2011;25(4):1891–9.
- [8] Wang G, Wang E, Huang Q, Li S. Effects of cationic and anionic surfactants on long flame coal seam water injection. *Fuel* 2022;309.
- [9] Abunowara M, Sufian S, Bustam MA, Eldemerdash U, Suleman H, Bencini R, Assiri MA, Ullah S, Al-Sehemli AG. Experimental measurements of carbon dioxide, methane and nitrogen high-pressure adsorption properties onto Malaysian coals under various conditions. *Energy* 2020;210:118575.
- [10] Xie W, Wang M, Chen S, Vandeginste V, Yu Z, Wang H. Effects of gas components, reservoir property and pore structure of shale gas reservoir on the competitive adsorption behavior of  $\text{CO}_2$  and  $\text{CH}_4$ . *Energy* 2022;254:124242.
- [11] Yang R, Liu S, Wang H, Lun Z, Zhou X, Zhao C, et al. Influence of  $\text{H}_2\text{O}$  on adsorbed  $\text{CH}_4$  on coal displaced by  $\text{CO}_2$  injection: implication for  $\text{CO}_2$  sequestration in coal seam with enhanced  $\text{CH}_4$  recovery ( $\text{CO}_2$ -ECBM). *Ind Eng Chem Res* 2021;60(43):15817–33.
- [12] Yutong F, Yu S.  $\text{CO}_2$ -Adsorption promoted  $\text{CH}_4$ -desorption onto low-rank coal vitrinite by density functional theory including dispersion correction (DFT-D3). *Fuel* 2018;219:259–69.
- [13] Weinberger B, Darkrim-Lamari F, Levesque D. Capillary condensation and adsorption of binary mixtures. *J Chem Phys* 2006;124(23):234712.
- [14] Wang S, Hu Y, Yang X, Liu G, He Y. Examination of adsorption behaviors of carbon dioxide and methane in oxidized coal seams. *Fuel* 2020;273:117599.
- [15] Du Y, Chen X, Li L, Wang P. Characteristics of methane desorption and diffusion in coal within a negative pressure environment. *Fuel* 2018;217:111–21.
- [16] Wu D, Liu X, Liang B, Sun K, Xiao X. Experiments on displacing methane in coal by injecting supercritical carbon dioxide. *Energy Fuels* 2018;32(12):12766–71.
- [17] Zhou K, Yang H, Guan J, Si Z. Study on the differences between various gas injection sources in the process of coal seam methane replacement by gas injection. *ACS Omega* 2022;7(42):37572–80.
- [18] Yue J, Wang Z, Shi B, Dong J, Shen X. Interaction mechanism of water movement and gas desorption during spontaneous imbibition in gas-bearing coal. *Fuel* 2022;318.
- [19] Kang N, Chen X, Yang H, Zhao S, Qi L. Effect of different placement sequences of water on the methane adsorption properties of coal. *ACS Omega* 2023;8(7):6689–98.
- [20] Dutta P, Bhownik S, Das S. Methane and carbon dioxide sorption on a set of coals from India. *Int J Coal Geol* 2011;85(3–4):289–99.
- [21] Dang Y, Zhao L, Lu X, Xu J, Sang P, Guo S, Zhu H, Guo W. Molecular simulation of  $\text{CO}_2/\text{CH}_4$  adsorption in Brown coal: effect of oxygen-, nitrogen-, and sulfur-containing functional groups. *Appl Surf Sci* 2017;423:33–42.
- [22] Zhou W, Wang H, Zhang Z, Chen H, Liu X. Molecular simulation of  $\text{CO}_2/\text{CH}_4/\text{H}_2\text{O}$  competitive adsorption and diffusion in Brown coal. *RSC Adv* 2019;9(6):3004–11.
- [23] Mosher K, He J, Liu Y, Rupp E, Wilcox J. Molecular simulation of methane adsorption in micro- and mesoporous carbons with applications to coal and gas shale systems. *Int J Coal Geol* 2013;109–110:36–44.
- [24] Yu S, Bo J, Jie-gang L. Nanopore structural characteristics and their impact on methane adsorption and diffusion in low to medium tectonically deformed coals: case study in the huaihai coal field. *Energy Fuels* 2017;31(7):6711–23.
- [25] Liu Y, Wilcox J. Molecular simulation studies of  $\text{CO}_2$  adsorption by carbon model compounds for carbon capture and sequestration applications. *Environ Sci Technol* 2013;47(1):95–101.
- [26] Liu Y, Wilcox J. Molecular simulation of  $\text{CO}_2$  adsorption in micro- and mesoporous carbons with surface heterogeneity. *Int J Coal Geol* 2012;104:83–95.
- [27] Zhang L, Aziz N, Ren T, Nemcik J, Tu S. Influence of coal particle size on coal adsorption and desorption characteristics. *Arch Min Sci* 2014;59(3):807–20.
- [28] Feng YY, Yang W, Chu W. Coalbed methane adsorption and desorption characteristics related to coal particle size. *Chin Phys B* 2016;25(6):068102.
- [29] Chen Y, Ma Z, Ma D, Zhang Z, Li W, Yang F, Ji Y, Peng T. Characteristics of the coal fines produced from low-rank coal reservoirs and their wettability and settleability in the binchang area, south ordos basin, China. *Geofluids* 2021;2021:1–17.
- [30] Qin C, Jiang Y, Fu Y, Chen S, Song X, Zuo S, Wu D, Zou N. Thermodynamic characteristics of high-pressure  $\text{CH}_4$  adsorption on longmaxi shale subjected to supercritical  $\text{CO}_2$ -water saturation. *Energy* 2023;263:125898.
- [31] Cui X, Yan H, Zhao P, Yang Y, Xie Y. Modeling of molecular and properties of anthracite Base on structural accuracy identification methods. *J Mol Struct* 2019;1183:313–23.
- [32] Zheng Z, Zhao F, Fu F, Zhang Y. Preparation of coal tar pitch based adsorption materials: understanding the adsorption mechanism by combining field energy theory and statistical physics models. *Chem Phys Lett* 2023;824:140564.
- [33] Hu H, Li X, Fang Z, Wei N, Li Q. Small-molecule gas sorption and diffusion in coal: molecular simulation. *Energy* 2010;35(7):2939–44.
- [34] Yu S, Bo J, Fengjuan L. Competitive adsorption of  $\text{CO}_2/\text{N}_2/\text{CH}_4$  onto coal vitrinite macromolecular: effects of electrostatic interactions and oxygen functionalities. *Fuel* 2019;235:23–38.

- [35] El Houda, Bensiradj N, Timón V, Boussassi R, Dalbouha S, Senent ML. DFT studies of single and multiple molecular adsorption of CH<sub>4</sub>, SF<sub>6</sub> and H<sub>2</sub>O in zeolitic-imidazolate framework (ZIF-4 and ZIF-6). *Inorg Chim Acta* 2019;490:272–81.
- [36] Rout A, Sahoo SS, Thomas S. Risk modeling of domestic solar water heater using Monte Carlo simulation for east-coastal region of India. *Energy* 2018;145:548–56.
- [37] Abu-Melha S Design. Synthesis and DFT/DNP modeling study of new 2-amino-5-arylazothiazole derivatives as potential antibacterial agents. *Molecules* 2018;23(2):434.
- [38] Zhang N, Zhang J, Wang G, Ning X, Meng F, Li C, Ye L, Wang C. Physicochemical characteristics of three-phase products of low-rank coal by hydrothermal carbonization: experimental research and quantum chemical calculation. *Energy* 2022;261:125347.
- [39] Chen YF, Su S, Liu T, Song YW, Wang X, Qing MX, Wang Y, Hu S, Zhang ZX, Xiang J. Microscopic mechanism and kinetics of NO heterogeneous reduction on char surface: a density functional theory study. *Energy* 2022;250:123861.
- [40] Yu B, Wang X, Iwahara J. Measuring local electrostatic potentials around nucleic acids by paramagnetic NMR spectroscopy. *J Phys Chem Lett* 2022;13(42):10025–9.
- [41] Gensterblum Y, Merkel A, Busch A, Krooss BM. High-pressure CH<sub>4</sub> and CO<sub>2</sub> sorption isotherms as a function of coal maturity and the influence of moisture. *Int J Coal Geol* 2013;118:45–57.
- [42] Qin C, Jiang Y, Cao M, Zhou J, Song X, Zuo S, Chen S, Luo Y, Xiao S, Yin H, Du X. Experimental study on the methane desorption-diffusion behavior of longmaxi shale exposure to supercritical CO<sub>2</sub>. *Energy* 2023;262:125456.
- [43] Chang CK, Tun H, Chen CC. An activity-based formulation for Langmuir adsorption isotherm. *Adsorption* 2020;26(3):375–86.
- [44] Tun H, Chen CC. Isosteric heat of adsorption from thermodynamic Langmuir isotherm. *Adsorption* 2021;27(6):979–89.
- [45] Pajdak A. Studies on the influence of moisture on the sorption and structural properties of hard coals. *Int J Greenh Gas Control* 2020;103:103193.
- [46] Wang Z, Su W, Tang X, Wu J. Influence of water invasion on methane adsorption behavior in coal. *Int J Coal Geol* 2018;197:74–83.
- [47] Zhou J, Xiong J, Ni J, Xie X, Liu Y. Structural changes and denitrification performance evaluation of bioretention cells with collapsible loess modified by coal gangue. *J Clean Prod* 2022;355:131740.
- [48] Singh A, Kumar D. Effect of temperature on elastic properties of CNT-polyethylene nanocomposite and its interface using MD simulations. *J Mol Model* 2018;24(7):178.
- [49] Ciftja O. Concise presentation of the coulomb electrostatic potential of a uniformly charged cube. *J Electrost* 2015;76:127–37.
- [50] Tsoi S, Dev P, Friedman AL, Stine R, Robinson JT, Reinecke TL, Sheehan PE. Van der Waals screening by single-layer graphene and molybdenum disulfide. *ACS Nano* 2014;8(12):12410–7.
- [51] Hao S, Wen J, Yu X, Chu W. Effect of the surface oxygen groups on methane adsorption on coals. *Appl Surf Sci* 2013;264:433–42.
- [52] Wang J, He Y, Peng Z, Ling X, Wang S. Estimation of hydrophilicity of coals by using the quantum Chemistry calculation. *Int J Miner Process* 2017;167:9–15.
- [53] Knak Jensen SJ, Tang TH, Csizmadia IG. Hydrogen-bonding ability of a methyl group. *J Phys Chem A* 2003;107(42):8975–9.
- [54] Fletcher AJ, Uygur Y, Thomas KM. Role of surface functional groups in the adsorption kinetics of water vapor on microporous activated carbons. *J Phys Chem C* 2007;111(23):8349–59.
- [55] Sakurovs R, Lewis C, Wibberley L. Effect of heat and moisture on surface titratability and pore size distribution of victorian Brown coals. *Fuel* 2016;172:124–9.